Article

Binding Mechanisms and Therapeutic Activity of Heterocyclic Substituted Arylazothioformamide Ligands and Their Cu(I) Coordination Complexes

Laxmi Tiwari, Caleb Leach, Ashley Williams, Brandon Lighter, Zachariah Heiden, Mark F. Roll, James G. Moberly, Kenneth A. Cornell,* and Kristopher V. Waynant*

Cite This: ACS Omega 2024, 9, 37141−37154

Read Online

ACCESS | Metrics & More | Article Recommendations | Supporting Information

ABSTRACT: Finding new sources of biologically active compounds for anticancer or antimicrobial therapies remains an active area of research. Azothioformamides (ATFs) with a 1,3 N=N−C=S heterodiene backbone are a new class of biologically active compounds that chelate metals (e.g., Cu) forming stable ATF metal coordination complexes. In this study, ATF ligands were prepared with pyrrolidine, piperidine, N-methylpiperazine, and morpholine substituents on the formamide as to add more heterocyclic drug-like character for biological studies. Formamide derivatives were then complexed with various Cu(I) salts to form coordination complexes. Cu(I) salts were selected as to create potential bioactive compounds with less toxicity. Binding association constants of each Cu(I) salt to ATF ligands were extrapolated from UV−vis titration studies and were corroborated with DFT calculations using a hybrid functional B3LYP method. It was observed that the smaller pyrrolidine functionalized ATFs bound to the Cu(I) salts had stronger binding than any of the larger six-membered-ring heterocycles with association values in the $10^4 - 10^5$ M^{-1} range. The ATF-Cu(I) salt coordination complexes were then evaluated for antimicrobial activity against two bacteria (*Staphylococcus aureus*, *Escherichia coli*), one yeast (*Candida albicans*), four human cancer lines (A-549, K-562, HT-1080, MDA-MB-231), and two normal human lines (MRC-5, HFF). The ATF ligands themselves were inactive against all microbes and most human lines except K-562 cells, which were sensitive to three of the four ligands (IC$_{50}$'s = 7.0−25.5 μM). Most ATF-Cu(I) complexes showed low to medium micromolar activity against *Candida albicans* (IC$_{50}$'s 2.6−24.8 μM) and *Staphylococcus aureus* (IC$_{50}$'s = 3.4−37.7 μM), with increasing activity corresponding to complexes with higher binding association constants. The antiproliferative properties of ATF-Cu(I) metal salt complexes against mammalian cells were mixed, with low to medium micromolar activity across all cell lines. Notably, several ATF-Cu(I) salt coordination complexes showed submicromolar activity against the HT-1080 fibrosarcoma line (0.52−0.69 μM). The results demonstrate promising activity of ATF-Cu(I) complexes, particularly with pyrrolidine as the formamide component. These studies suggest that the stronger binding association values correlate to higher levels of biological activity.
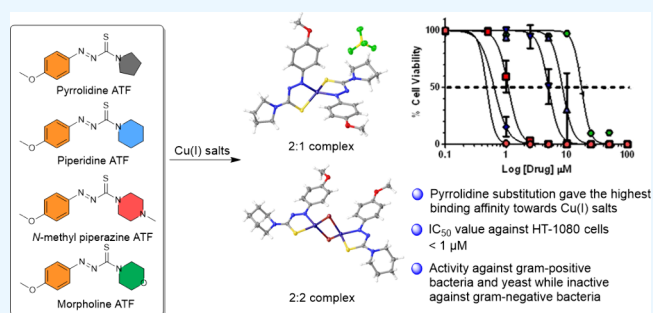
INTRODUCTION

Copper is an essential micronutrient for all living organisms and while Cu(II) is the predominant oxidation state in blood, reduced Cu(I) is more common intracellularly.[1,2] Copper also plays a complex role in cancer, with increased concentrations both stimulating angiogenesis and the production of chelators that disrupt tumor growth.[3] Given the essential function of copper in both healthy and cancerous cells, there is great interest in finding druggable mechanisms of action as well as potential therapeutics that target its involvement in cellular processes. Experimental evidence suggests that increased copper levels induce cytotoxicity through reactive oxygen species (ROS) formation.[4] Other proposed mechanisms include DNA intercalation or chelation systems that deliver apoptotic doses of copper into the cell.[3] Both the ligands and

their copper chelates in chelation delivery systems, have been the subject of thorough investigation for biological activity against a range of microbes and cell lines, but with mixed results.[5] In terms of ligands, the thiosemicarbazones (TSCs) are particularly active both as metal(I) and both as metal(I) and metal(II) with fewer examples.[6−13] For example, triapine (Figure 1, **3-AP**), is a known iron and copper chelator that
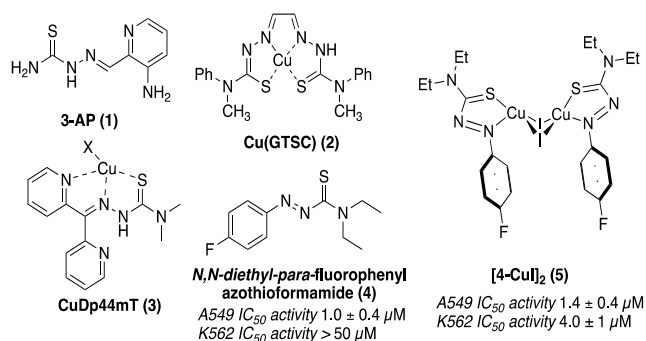
Figure 1. Representative examples of thiosemicarbazones (3-AP), copper-coordinated thiosemicarbazones (Cu[GTSC]; CuDp44 mT), azothioformamide (F-ATF), and copper coordinated azothioformamide ([[(F-ATF)-CuI]₂]) that exhibit anticancer and/or antimicrobial activity.

works with glutathione to modulate ROS levels in the cell.[14,15] Triapine has undergone numerous studies against various cancer cell lines and is now in phase II and III clinical trials.[16,17] Copper-coordinated thiosemicarbazones, including **CuGTSC** and **CuDp44 mT** (Figure 1), exhibit submicromolar activity against numerous cancer lines in *in vitro* and *in vivo* studies.[18,19] Azothioformamide (ATF) ligands (i.e., **F-ATF**, Figure 1), have similar core structures to TSCs but utilize a fully conjugated 1,3 N=N—C=S heterodiene binding motif in the metal chelation. In a preliminary study, ATF ligands demonstrated activity against the A549 lung carcinoma cell line (IC_{50} = 1–10 μM), yet showed no activity against K562 human leukemia cells (IC_{50} > 100 μM).[20] However, resultant Cu(I) complexes (i.e., [(**F-ATF**)-**CuI** Figure 1) of these same ATF ligands showed low (1–10 μM) to moderate (10–50 μM) IC_{50} values against both K562 and A549 cells, perhaps indicating multiple mechanisms of action for these complexes. Many examples of copper induced cytotoxicity have utilized both Cu(I) and Cu(II) coordination complexes and therefore the use of a redox-active ligand could promote multiple apoptotic mechanisms.[15,21–24]

Redox-active ATF ligands were first reported in the 1970s and have been utilized as ligands for the mild oxidative dissolution of late transition metals and applied to the removal of trace metals from various polymeric materials.[25–27] In these resultant 2:1 ligand to metal complexes, the copper is oxidized to Cu(II) and the ATF ligands are singly reduced. However, when ATFs are mixed with oxidized metal salts, specifically Cu(I), the coordination remains neutral with X-ray crystal structures showing either dimeric 1:1 coordination complexes (producing 2:2 dimers, i.e., [(**F-ATF**)-**CuI**]₂) or 2:1 ligand: metal coordinative structures, depending on the source of the

metal salt (i.e., Cu(I) halides or tetrakisacetonitrile Cu(I) tetrafluoroborate/hexafluorophosphate, respectively).[28–31] UV−vis titration studies of ATFs, containing either alkyl and aryl substituents with appended electron-donating groups (EDG) or electron-withdrawing groups (EWG) have produced binding association constants that ranged from 1,000−30,000 M^{-1}, depending on the substitution pattern. EDG appended compounds exhibited the strongest binding with Cu(I) salts when a series of ATFs with varying EDG/EWG substitution was evaluated, corresponding to decreasing electronic strength at the *para*-position (OMe > CH_3 > F > CF_3).[29] Subsequently, a study on the placement of the EDG aryl substitution, (i.e., *para, meta, and ortho* methoxy) concluded with the *para* substituted compounds exhibiting higher binding associations compared to *ortho* and *meta* substituted compounds, suggesting a steric interaction influencing the binding of the metal.[30] Interestingly, all complexes including the 2:2 dimers fit better to a 2:1 binding model rather than the 1:1 binding model, which suggests the possibility of multiple binding mechanisms.[29]

Since the electronic characteristics of the aryl ring alter the metal binding capabilities of the ATF, this report focuses on the importance of the thioformamide component of the ATF for both binding and resultant biological activity. The contribution of the C−N bond distances and angles in the thioformamide heterocycles are particularly important. Thioformamides have already been established as having greater nitrogen to sulfur charge transfer and larger rotational barriers over amides.[32] Cyclic amides further limit the rotation, and mixed heterocycles add hydrogen bond accepting atoms (i.e., morpholine) that may either inhibit or enhance binding to target atoms or molecules in the cell. Herein, a series of ATFs were synthesized with variable symmetric heterocyclic formamide groups as the secondary amine: (pyrrolidine, piperidine, *N*-methylpiperazine, and morpholine). Based on prior work and to ensure strong associative binding to Cu(I), the electron donating *para*-substituted methoxy group was used for all aryl substitutions. A previous study synthesized and examined ATFs with pyrrolidine heterocycles complexed to Cu(II), Ni(II), and Zn(II), but did not explore the metal(I) salt coordination nor their biological activity.[33] Recently a similar pyrrolidine substituted azoformamide ligand was synthesized and coordinated to Zn(II) but has yet to be tested for therapeutic activity.[34] It was hypothesized that a decreased binding trend would be found through the additional bulk and electrostatics of larger heterocycles, yet their additions, because of their relevance in common therapeutics, could favorably affect the biological activity when compared to the previously studied *N,N*-diethyl MeOATF.[20] When compared to other active metal−ligand
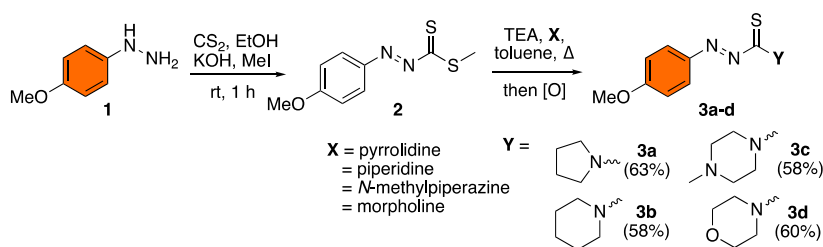
Figure 2. Synthetic scheme for heterocyclic para-methoxyphenylazothioformamides containing pyrrolidine (**3a**), piperidine (**3b**), *N*-methylpiperazine (**3c**), and morpholine (**3d**) substituents.
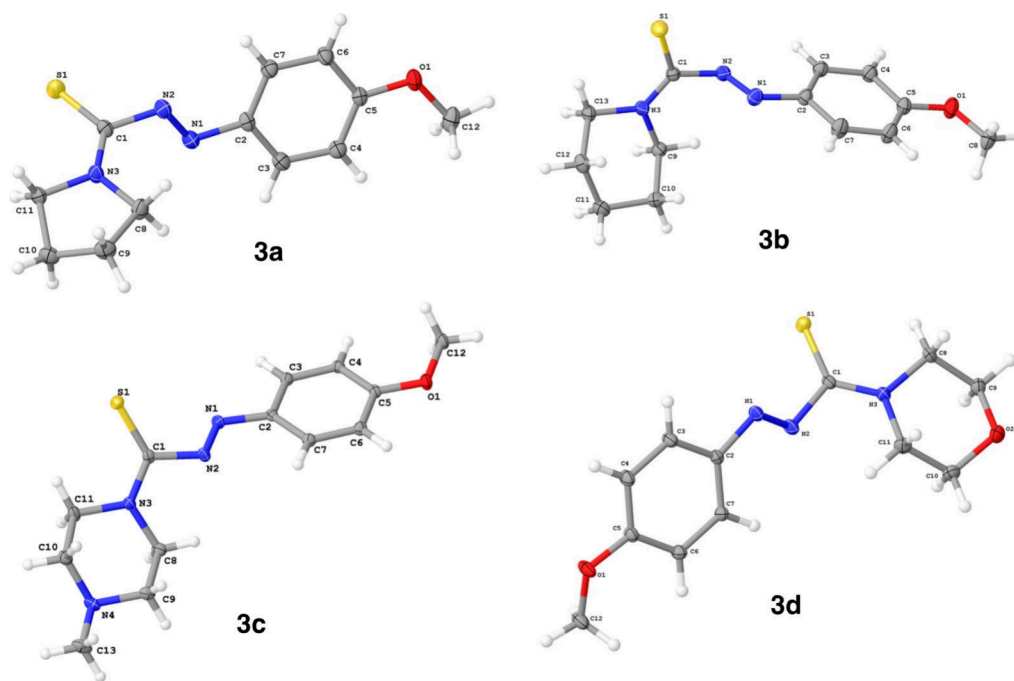
Figure 3. X-ray crystal structures for **3a**−**3d**. All crystal structures are shown at 50% thermal ellipsoid probability.

Table 1. Bond Distances and Angles for Substituted ATF Ligands from Single-Crystal X-ray Diffraction

	Bond Distances (Å)					Bond Angles				
Ligand	$N_1=N_2$	N_2-C_1	$C_1=S_1$	C_1-N_3	C_2-N_1	N1−N2−C1	N2−C1−S1	N2−C1−N3	S1−C1−N3	C2−N1−N2
Pyrrolidine p-MeO ATF (**3a**)	1.2529(19)	1.4404(9)	1.6654(16)	1.3169(19)	1.4209(16)	110.97	116.65	116.93	126.33	114.3
Piperidine p-MeO ATF (**3b**)	1.2524(17)	1.4361(17)	1.6679(14)	1.3228(18)	1.4229(18)	113.1	117.27	114.52	127.94	114.78
N-methyl piperazine p-MeO ATF (**3c**)	1.2582(11)	1.4420(12)	1.6636(9)	1.3312(12)	1.4102(12)	112.23	119.32	113.62	126.81	115.78
Morpholine p-MeO ATF (**3d**)	1.2514(15)	1.4338(16)	1.6664(13)	1.3281(16)	1.4209(16)	114.1	119.39	113.51	126.81	114.35
N,N-diethylamino-p-MeO ATF[a]	1.257(7)	1.435(8)	1.670(6)	1.3277(15)	1.4223(15)	113.89	117.74	114.74	127.27	114.72

[a]These values were obtained from a previous report.[29]

compounds, it was proposed that the stronger metal binding affinities would provide greater biological activity than that exhibited by the ligands alone. Herein we continue to investigate the properties of ATF-Cu(I) complexes and explore the role of additional heterocyclic substituents to the formamide moiety to establish structure−activity relationships and begin to identify potential mechanisms of action of their biological activity. With limited preliminary reports on the antiproliferative properties of ATF-Cu(I) complexes, a general antimicrobial and anticancer investigation was undertook. The results continue to support the further study of these ATF-Cu(I) complexes as promising antibiotics and anticancer therapeutics.

■ RESULTS AND DISCUSSION

Synthetic Chemistry. The known one-pot synthesis of ATF ligands[26,28] required modification to produce **3a**−**d** in decent yields. Xanthate ester intermediate, **2**, as shown in Figure 2, was isolated (79% yield) to limit side products. The xanthate intermediate is then reacted with the heterocyclic secondary amine in 1.1 stoichiometric equivalents (and not as the solvent) using toluene to increase reflux temperatures and an equivalent of triethylamine was added to help push the reaction to completion. Following air oxidation, ligands **3a**−**d**, were concentrated, chromatographed, and recrystallized using

the slow evaporation method. X-ray crystal structures are shown in Figure 3. All ligands were characterized with NMR, FTIR, mass spec, melting point, and UV−vis max absorbance (all characterization data can be found in the electronic Supporting Information, ESI). Spectroscopically, the ligands produce similar NMR, FTIR and UV−vis spectra with extinction coefficients for **3a**−**3d** from 2.8×10^4 M^{-1} cm^{-1} − 1.7×10^4 M^{-1} cm^{-1}.

Key distances and angles of ligands **3a**−**d** (shown in Figure 3) are noted in Table 1. Further XRD data on **3a**−**d** can be found in ESI Figures S43−46. Compounds **3a**, **3b**, and **3d** have triclinic crystal systems with a P-1 space group whereas **3c** has monoclinic crystal system and P2$_1$/n space group. Details concerning crystal data and refinement are given in ESI Table S4. Bond lengths for N=N, C=S, N−C and chelation specific bond angles for various substituted ATFs are noted in Table 1 displaying similar bond lengths and angles of previously reported ATFs.[29] Overall, the N1−C1−N3 bond angles for all ligands are between 113 and 117° showing nearly planar sp^2 hybridized behavior at C$_1$. The torsion angle for *N*-methyl piperazine derivative **3c** of C2−N1−N2−C1 is 175.02° and S1−C1−N2−N1 is −55.03°. When compared to previously reported *N,N*-diethylamino-*p*-MeO-ATF, we find that the key bond distances are very similar to **3a** but the bond angles are
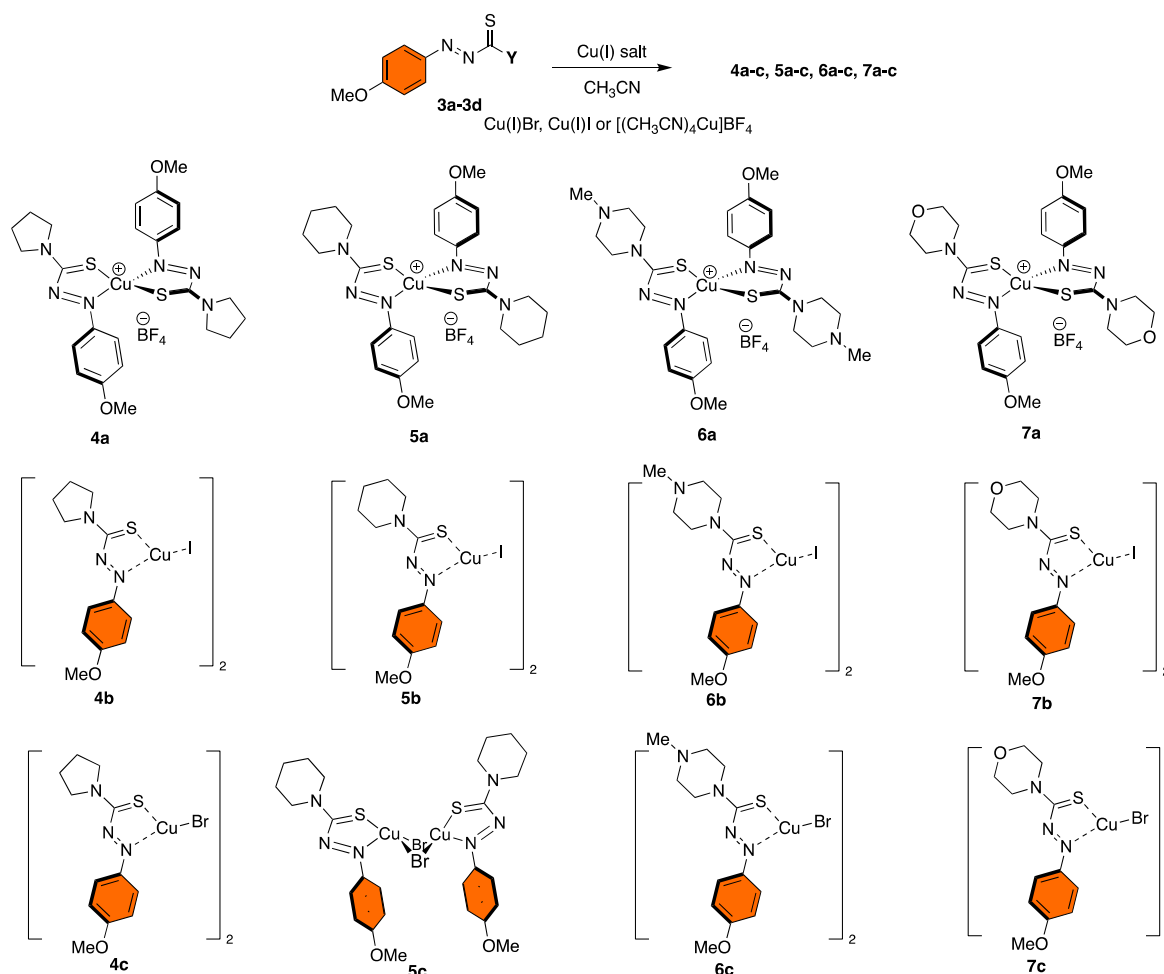
Figure 4. Copper(I) coordination complexes of the various formamide ligands.
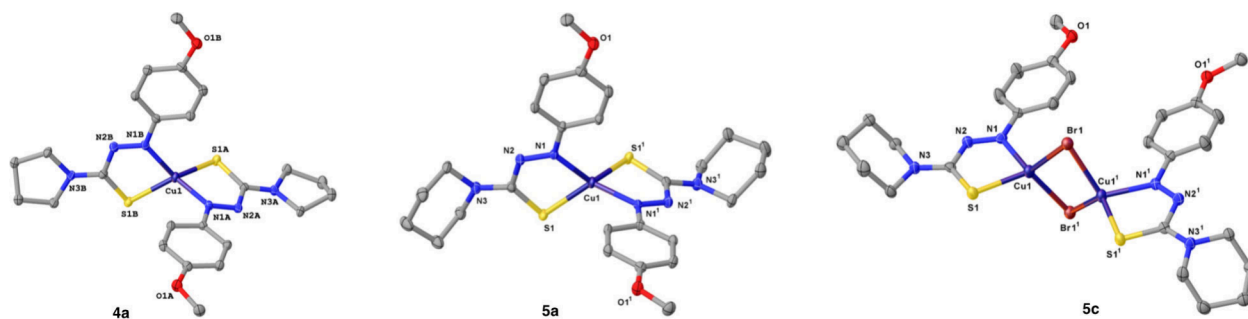

Figure 5. X-ray crystal structures for **4a**, **5a**, and **5c**. For **4a** and **5a**, the BF$_4$ counterion has been removed for clarity. In all cases the ligands exhibit neutral coordination. All thermal ellipsoids are shown with 50% probability.

Table 2. Bond Distances and Angles for Selected ATF-Metal Complexes from Single-Crystal X-ray Diffraction

|	Bond Distances (Å)					Bond Angles				
Complex	N$_1$=N$_2$	N$_2$–C$_1$	C$_1$=S$_1$	C$_1$–N$_3$	N$_1$–Cu	S$_1$–Cu	N1–N2–C1	N2–C1–S1	N2–C1–N3	S1–C1–N3	S1–Cu–N1
4a	1.275	1.417	1.696	1.316	2.001	2.284	114.57	124.53	111.47	124.01	85.59
5a	1.270	1.418	1.695	1.324	2.001	2.274	114.86	123.1	112.06	124.76	85.10
5c	1.273	1.427	1.692	1.334	2.051	2.303	115.1	123.57	111.53	124.89	83.87

more similar to the bulkier **3b** and binding association constants are found to be in between the two.[29]

Ligands **3a**–**3d** were then reacted with Cu(I) salts (CuBr, CuI, and [(CH$_3$CN)$_4$Cu]BF$_4$) using acetonitrile as solvent at 50 °C as shown in Figure 4. Following concentration and

subsequent washing, coordination complexes were obtained yielding complexes **4a**–**7c** in decent yields of 42–75%. All complexes were fully characterized with NMR, FTIR, elemental analysis, and melting point (see ESI). Structures shown in Figure 4 are either based on confirmed crystal
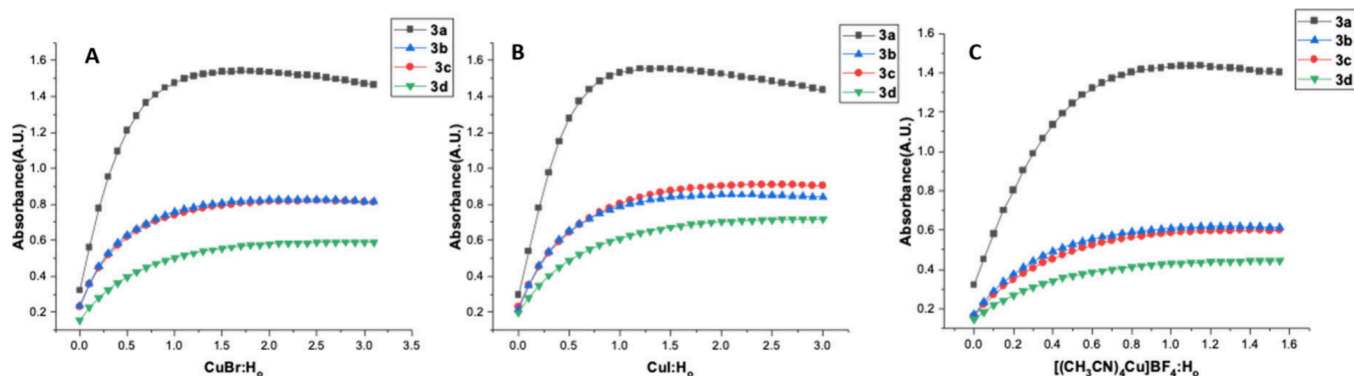
Figure 6. Binding isotherms of ATF ligands at comparable wavelengths for the titration of A) Cu(I)Br; B) Cu(I)I; and C) $[(CH_3CN)_4Cu(I)]BF_4$ (all measurements were performed in triplicate).
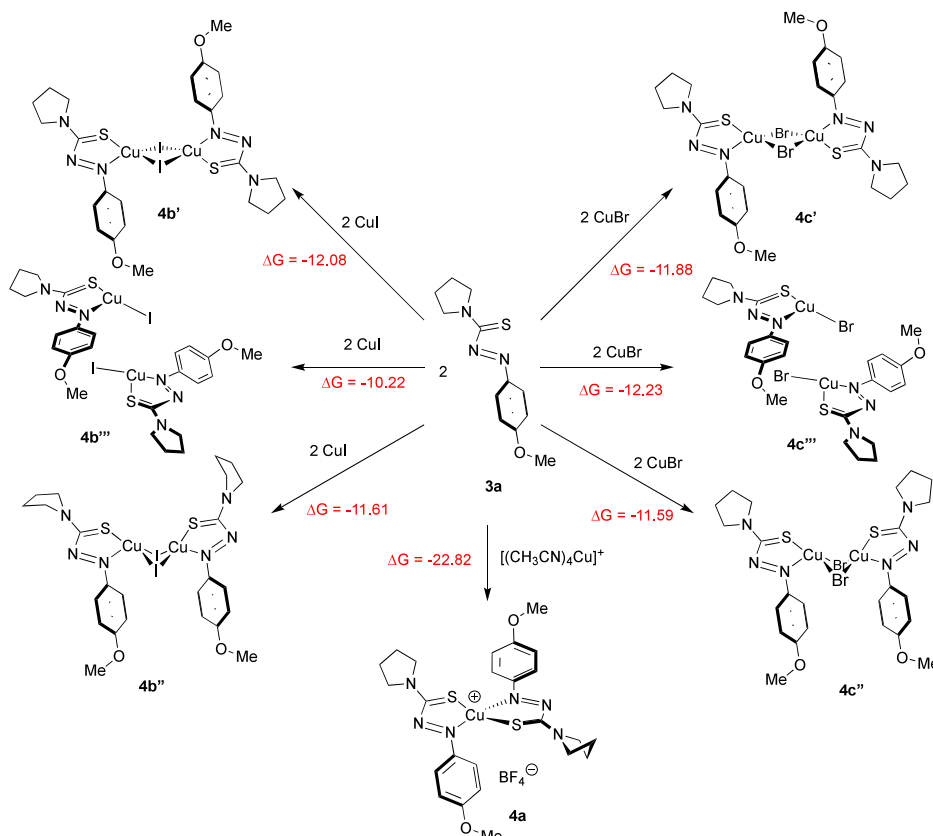
Figure 7. Example structures based on the Gibb's free energy calculations of ligand **3a** bound to Cu(I) iodide (**4b**), Cu(I) bromide (**4c**), and Cu(I) tetrafluoroborate (**4a**) salts in kcal/mol.
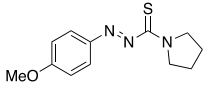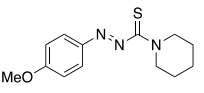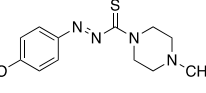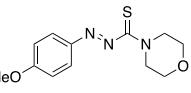
structure determinations (**4a**, **5a**, and **5c**, shown below in Figure 6), or are based on modeled 2:1 complexes (**6a**, **7a**) or 2:2 complexes that can form in a variety of conformations (i.e., *exo*-X dimer, *μ*-X dimer) and are therefore indicated with a bracket, [ ] (i.e., **4b**, **4c**, **5b**, **6b**, **6c**, **7b** and **7c**). ^1H and ^{13}C NMR data (ESI Figures S11−34) show downfield shifts of both the aryl and the formamide substituents upon metal(I) coordination.

Recrystallization via slow evaporation and/or mixed solvent systems was attempted with all metal−ligand complexes and yet successful for **4a**, **5a**, and **5c** with single crystal X-ray crystal structures shown in Figure 5. Bond distances are noted in Table 2 and all experimental crystal data can be found in ESI

(Figures S47 − S49). Bond distances and angles were comparable with previously found structures.[20,30,31,35]

Coordination and Binding Studies. Binding isotherms are shown in Figure 6 and were generated from UV−vis titration data, which can be found in the ESI, Figures S40−42. The isotherms highlight an increase in binding affinity for the pyrrolidine substituted azothioformamide over all other heterocycles measured in this study and an increased affinity over previously reported N,N-diethyl appended azothioforma-mide.[29] The binding association constants found ranged from 10^4 M^{-1} to 10^5 M^{-1} and correlated best (least error) with full, noncooperative, and statistical 2:1 model types that utilize multiple degrees of freedom in the calculations (Binding Association Data can be found in ESI (Tables S2−S3).[36,37]

Table 3. IC$_{50}$ Values for ATF Ligands

		Compound IC$_{50}$, µM (± SEM)			
		3a	**3b**	**3c**	**3d**
Microbe:	S. aureus	>50	>50	>50	>50
	E. coli	>50	>50	>50	>50
	C. albicans	>50	>50	>50	>50
Cell line:	A549	>50	>50	>50	>50
	HT-1080	>50	>50	>50	>50
	MDA-MB-231	>50	>50	49.2 (0.8)	>50
	K-562	7.0 (0.3)	25.5 (0.5)	11.0 (0.3)	>50
	MRC-5	>50	>50	>50	>50
	HFF	>50	>50	>50	>50

These data support previous reports of a 2:1 binding mechanism for 2:2 dimeric coordination complexes (i.e., **4a**–**7c**), which suggests a precoordinated dimeric metal salt prior to ligand binding.[30] The binding strength for pyrrolidine-*p*-MeO-ATF, (**3a**), was three times stronger than *N*-methyl piperazine-*p*-MeO-ATF, (**3c**), and piperidine-*p*-MeO-ATF, (**3b**), and approximately four times stronger than morpholine-*p*-MeO-ATF, (**3d**). Similarly, the molar extinction coefficient of pyrrolidine-*p*-MeO-ATF, (**3a**), is highest among all heterocycles and has around 1.5 times stronger binding affinity than the previously reported 4-methoxy-*N,N*-diethyl-ATF.[29] The strong binding for pyrrolidine-*p*-MeO-ATF, (**3a**), is believed to be due to the sterically locked pyrrolidine allowing for the ligand to coordinate faster.

To note, is that the bond distances and bond angles of (**4a**) and (**5a**), as found in the XRD data above (Table 2), were very similar, whereas binding association was found to be much higher for pyrrolidine than piperidine. Therefore, an increase in binding can be more correlated with the decreased steric interactions and mobility of the pyrrolidine functionalized ligand with the Cu(I) salt over the six-membered heterocycles. Similarly, the angles and distance correlations between (**5a**) and (**5c**) also compare quite well. Notably, the Cu–Cu distance in the 1:1 dimer was found to be 2.947 Å and the Cu–Br distance was 2.441/2.476 Å, respectively. As ATF ligands are redox-active, therefore cyclic voltammetry (CV) was performed and CV of all ligands and complexes are reported in the ESI (Figure S53–56) along with noted oxidations/reductions in Table S6.

Computational Studies. Metal to ligand associations were optimized using a hybrid functional B3LYP method and are based on B3LYP/6-311++G(d,p) electronic energies and all corrections calculated at the B3LYP/6-31 G(d) level. These free energies were then utilized to calculate the equilibrium constants to compare these values with the experimental results. Cu(I) halides can form 2:2 complexes with ATF ligands as either *µ*-X dimers or as *µ*-X butterfly dimers (i.e., **4b'** and **4c'**). Interestingly, metal-ATF complexes have yet to be experimentally isolated as simple 1:1 complexes, although computationally these 1:1 structures are favored. However, each of these orientations were computationally studied (in

acetonitrile), with varying results for specific formamide substitutions. Shown below in Figure 7 are all the possible structural orientations of **3a** when complexed with Cu(I) salts and the most favored structures based on the results of the lowest Gibb's free energy (Δ*G*°) calculations for three 2:2 dimers that have been found previously including the *µ*-X dimer (i.e., **4b'**, **4c'**) and the *µ*-X butterfly dimer (i.e., **4b'''**, **4c'''**) with either Cu(I)I or Cu(I)Br, respectively. The orientations found as **4b"** and **4c"** are similar to the found *exo*-X dimers seen previously but yet are not predicted to dimerize in this study.[30] Also shown is ligand **3a** modeled with [(CH$_3$CN)Cu]$^+$ to form 2:1 complex, (**4a**), which exhibits a strong exergonic preference. Corresponding calculations for all other complexes from the various formamide substitutions are shown in ESI (Figure S50–52). The results of the calculated Gibbs Free Energy (Δ*G*°) binding constants for the ligands (ESI, Table S5) indicate that the pyrrolidine ATF ligand (**3a**) has the highest rate constant, k, which correlates well with the binding titration experiments shown above in Figure 4. A trend correlating the size and electrostatics of the heterocycles was not found yet they were all favorable with positive rate constants.

Biological Activity. ATFs were evaluated using a microdilution assay as previously described.[10] The ATFs were tested against three microbial species: *Staphylococcus aureus* (MRSA, ATCC BAA-44), *Escherichia coli* (ATCC 8739), and the yeast *Candida albicans* (ATCC 10231) to begin to investigate potential effects in different cell wall biotypes. Minimum inhibitory concentration (MIC) values can be found in ESI (Table S7). Similar to our prior reported results,[16] ATFs showed no appreciable antimicrobial activity against all three microbial species (IC$_{50}$'s > 50 µM) (Table 3). ATFs were also examined using a resazurin antiproliferative microdilution assay as previously described[16] and were screened against four human cancer cell lines: adherent A549 lung adenocarcinoma, adherent HT-1080 fibrosarcoma, adherent MDA-MB-231 breast adenocarcinoma, and nonadherent K-562 chronic myelogenous leukemia; and two human noncancerous cell lines: adherent MRC-5 lung fibroblasts and adherent HFF foreskin fibroblasts. As shown in Table 3, ATFs overall showed no appreciable biological activity except toward K-562 cells,

which were sensitive to **3a**, **3b**, and **3c**. In this report, we did not observe low micromolar ATF inhibition of A549 cells, which was seen in our previous report.[16] The difference in ATF biological activity for A549 cells is unclear, but these findings indicate ligand specificity is essential for impacting an A549 cellular target.

The antimicrobial results of the ATF-metal chelating complexes, **4a−7c**, are presented in Tables 3-7 with

Table 4. IC$_{50}$ Values for Pyrrolidine ATF-Metal Chelating Compounds

		Compound IC$_{50}$, μM (± SEM)		
		4a	**4b**	**4c**
Microbe:	S. aureus	21.1 (6.7)	3.4 (0.8)	4.1 (0.1)
	E. coli	>50	>50	>50
	C. albicans	>50	5.0 (2.6)	2.7 (0.7)
Cell line:	A549	20.8 (1.8)	12.7 (1.7)	3.5 (0.7)
	HT-1080	10.0 (1.8)	0.52 (0.04)	1.1 (0.7)
	MDA-MB-231	14.9 (3.1)	4.0 (0.6)	3.2 (0.9)
	K-562	16.3 (3.3)	1.2 (0.1)	9.6 (3.9)
	MRC-5	18.0 (1.1)	1.5 (0.4)	9.6 (1.1)
	HFF	19.6 (3.8)	5.6 (1.2)	3.9 (0.8)

Table 5. IC$_{50}$ Values for Piperidine ATF-Metal Chelating Compounds

		Compound IC$_{50}$, μM (± SEM)		
		5a	**5b**	**5c**
Microbe:	S. aureus	7.9 (0.2)	12.4 (1.4)	8.5 (1.5)
	E. coli	>50	>50	>50
	C. albicans	3.2 (0.6)	8.9 (2.8)	2.6 (0.8)
Cell line:	A549	5.3 (0.2)	12.2 (1.4)	2.4 (0.5)
	HT-1080	7.6 (1.1)	4.9 (0.4)	0.69 (0.03)
	MDA-MB-231	4.8 (1.6)	11.1 (1.1)	4.5 (1.0)
	K-562	10.4 (2.3)	13.1 (1.4)	1.8 (0.5)
	MRC-5	7.8 (2.0)	14.9 (3.8)	3.3 (0.3)
	HFF	10.3 (0.4)	13.6 (4.5)	1.5 (0.4)

Table 6. IC$_{50}$ Values for N-Methylpiperazine MeOATF-Metal Chelating Compounds

		Compound IC$_{50}$, μM (± SEM)		
		6a	**6b**	**6c**
Microbe:	S. aureus	14.0 (1.5)	9.8 (0.7)	9.8 (1.5)
	E. coli	>50	>50	>50
	C. albicans	24.8 (5.4)	21.8 (2.3)	14.3 (2.0)
Cell line:	A549	10.2 (0.4)	21.1 (0.6)	11.6 (1.5)
	HT-1080	9.1 (0.7)	13.5 (0.8)	13.1 (1.5)
	MDA-MB-231	8.2 (0.7)	3.5 (0.8)	10.9 (0.6)
	K-562	6.6 (0.6)	1.8 (0.5)	8.1 (1.3)
	MRC-5	8.1 (1.2)	2.4 (0.5)	9.2 (1.6)
	HFF	7.8 (1.4)	2.7 (0.4)	12.3 (2.0)

Table 7. IC$_{50}$ Values for Morpholine ATF-Metal Chelating Compounds

|		Compound IC$_{50}$, μM (± SEM)		
		7a	**7b**	**7c**
Microbe:	S. aureus	7.8 (2.2)	37.7 (5.2)	9.9 (2.0)
	E. coli	>50	>50	>50
	C. albicans	9.6 (1.6)	>50	14.1 (1.4)
Cell line:	A549	8.5 (1.1)	3.2 (0.6)	2.0 (0.1)
	HT-1080	6.7 (0.4)	9.1 (1.6)	19.6 (4.4)
	MDA-MB-231	3.2 (0.3)	3.0 (0.5)	2.1 (0.1)
	K-562	3.9 (0.2)	4.5 (0.8)	15.6 (2.9)
	MRC-5	4.5 (0.4)	4.0 (0.1)	3.2 (0.1)
	HFF	8.8 (0.3)	6.0 (1.3)	5.6 (0.4)
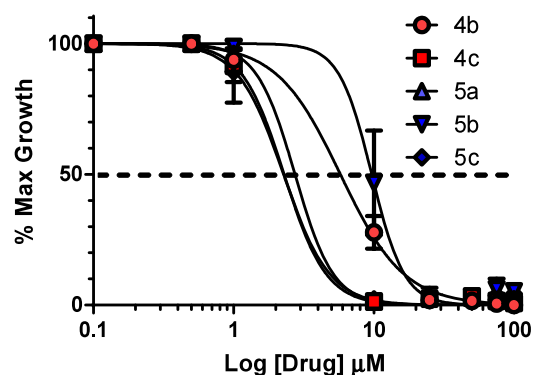
Figure 8. IC$_{50}$ curves of ATF-metal chelating complexes against *Candida albicans*.

(1−10 μM) to moderate (10−50 μM) micromolar activity, but no growth inhibition was observed for the Gram-negative *Escherichia coli* (IC$_{50}$'s > 50 μM). The difference in activity observed between Gram-positive and Gram-negative bacteria in this study suggests that the ATF-metal chelating complexes may interfere with the accessible peptidoglycan cell wall biosynthetic machinery present in the membrane of Gram-positive bacteria. However, these large molecular weight metal complexes may be impermeable to the outer membrane of Gram-negative bacteria, and thus unable to access the cell wall biosynthetic machinery. Like Gram-positive *Staphylococcus*, *Candida albicans* also has an outer cell wall, but it is composed of β-1,3-glucans, β-1,6-glucans, and chitin rather than peptidoglycan.[20] ATF-metal chelating complexes could also be interacting with the β-glucan-chitin skeleton of the *Candida albicans* cell wall or impacting the activity of β-glucan and/or chitin synthases. Alternatively, copper, and other transition metal complexes are known to be redox active and may affect their cytotoxic effects through DNA cleavage that occurs through either direct DNA binding redox reactions, or through generation of reactive oxygen species or other radicals that modify the DNA.[38] The generation of reactive oxygen and radical species may also lead to membrane lipid peroxidation that alters membrane permeability or leads to altered membrane potential. In any case, these potential mechanisms of action are still largely conjecture and future studies will be important for determining the exact biochemical event(s) for ATF-Cu(I) complex activity in microbial and mammalian cells.

Interestingly, the antimicrobial activity of the pyrrolidine appended ATF ligand was increased when complexed with

representative growth inhibition curves presented in Figure 8. The Gram-positive multidrug resistant *Staphylococcus aureus* and eukaryotic *Candida albicans* were both found to be susceptible to the metal salt coordination complexes with low

Cu(I) iodide and bromide salt complexes (**4b**, **4c**) compared to the Cu(I) tetrafluoroborate complex (**4a**). Considering the differences in free energy between these compounds, it could indicate that the affinity for copper ion is an essential characteristic for its antimicrobial activity. In other cases, the Cu(I)-ATF piperidine and morpholine tetrafluoroborate coordination complexes (**5a**, **7a**) outperformed the activity of the corresponding Cu(I)I and Cu(I)Br salt (**5b**, **5c**, **7b**, **7c**), indicating that the contribution of the counterion to antimicrobial activity was complex. However, we also observed that as the binding affinity of the ATF decreased (**4b** pyrrolidine [47,243 M^{-1}] ≫ **5b** piperazine [6,904 M^{-1}] > **6b** N-methylpiperazine [5,496 M^{-1}] > **7b** morpholine [3,915 M^{-1}]) that the effectiveness of the complexes containing iodide as the counterion decreased. A similar trend was also observed for the Cu(I)Br complexes, although it was not always consistent with binding affinity. We hypothesize that as a whole; the ATF metal salt coordination complexes could be improved as antimicrobial agents by increasing the binding affinity of the ATF ligand to its metal center.

The antiproliferative properties of the ATF metal chelates against an array of normal human and cancer cell lines can be seen in Figure 9 and are summarized in Tables 4-7. Generally,
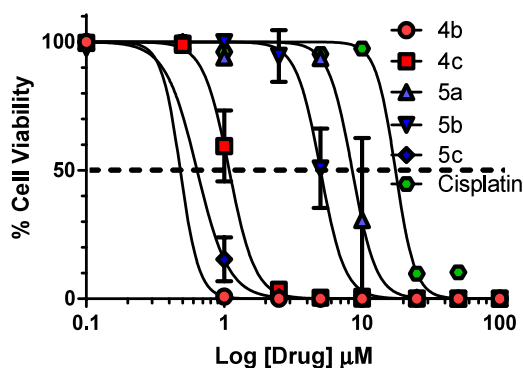
Figure 9. IC$_{50}$ curves of ATF-metal chelating complexes against HT-1080 fibrosarcoma cells.

the ATF ligands alone showed poor activity against the majority of cell types. However, the ATF-Cu(I) complexes showed low micromolar (IC$_{50}$ = 1−10 μM) to moderate micromolar (IC$_{50}$ = 10−50 μM) across all of the normal human cells and human cancer cell lines. Of note, the HT-1080 fibrosarcoma cell line was particularly sensitive at submicromolar concentrations of complexes **4b** (IC$_{50}$ = 0.52 μM), **4c** (IC$_{50}$ = 1.1 μM), and **5c** (IC$_{50}$ = 0.69 μM), which may be of interest due to the limited arsenal of therapeutics for sarcomas. Against HT-1080 cells, the activity of the Cu(I) halide complexes also improved with increasing ligand binding affinity (Figure 9) and showed more potent activity than cisplatin (IC$_{50}$ = 17.5 μM). Similar to the antimicrobial results, the pyrrolidine appended ATF ligand also showed increased activity when complexed with Cu(I) halide metal centers (**4b**, **4c**). Otherwise, there were generally only modest or insubstantial differences in activity based in the metal center or ATF ligand seen across the mammalian cells. The exact antiproliferative mechanism of ATF metal chelates is unknown, but our studies suggest that the combination of the metal center and ATF ligand heavily influences *in vitro* biological activity. Future studies will explore possible mechanisms including cuproptosis,[21] reactive oxygen species (ROS)

production,[22] inhibition of type II topoisomerase (which has been reported for related metal-thiosemicarbazones),[23] redox dependent DNA cleavage, and membrane instability (permeabilization, depolarization).[38−40]

CONCLUSIONS

A small library of azothioformamide (ATF) ligands with various formamide heterocycles and their Cu(I) coordination complexes have been synthesized and evaluated for therapeutic activity. Results from the synthesis, experimental and computational coordination studies, along with the biological evaluation of these ATF and ATF-Cu(I) complexes revealed that the smaller ring size (pyrrolidine) of the formamide component on the ligand produced the strongest binding association constants. Against certain cell lines, the pyrrolidine appended Cu(I) halide structures also elicited higher antimicrobial biological activity (i.e., **4b**, **4c**, etc.), while the antineoplastic activity was independent of the combination of the Cu(I) and ATF ligand type. Furthermore, ATF ligands themselves were inactive against all microbes and most of the cancer cell lines with **3a** being slightly active against cancer cell line K-652 with a relatively low IC$_{50}$ value (7.0 μM). However, ATF-Cu(I) coordination complexes showed highly contrasting effects against the microbial strains. The Gram-positive bacteria *Staphylococcus aureus*, which displays a multidrug resistance phenotype due to the expression of a drug efflux pump, was sensitive to most of the ATF-Cu(I) complexes. Similarly, the yeast *Candida albicans* showed sensitivity across many of the ATF-Cu(I) complexes, with the most uniform activity (IC$_{50}$ = 2−9 μM) exerted by the piperidine appended ATF complexes. The Gram-negative bacteria *E. coli* was uniformly insensitive to the compounds. In the cancer cell line antiproliferative studies, the ATF-Cu(I) complexes were active against all the cell lines tested with complexes **4b** and **5c** being very active with IC$_{50}$ values <1 μM against HT-1080 cells. Further studies are needed to thoroughly distinguish the mechanism(s) of action of these complexes against bacteria, yeast, and mammalian cells.

EXPERIMENTAL SECTION

Materials and Methods. All reagents were purchased from quality commercial sources and used without purification. Methyl iodide was purchased from EMD Millipore, 4-methoxyphenyl hydrazine hydrochloride was purchased from AK Scientific (Union City, CA); pyrrolidine, piperidine, morpholine, N-methyl piperazine, carbon disulfide and common solvents were purchased from ThermoFisher; Cu(I) halides and salts were purchased from ThermoFisher, Millipore-Sigma, and AK Scientific. ^{1}H and ^{13}C NMR experiments were performed on a Bruker AVANCE 300 and 500 MHz using either CDCl$_3$, DMSO-d_6, or CD$_3$CN as solvent and referenced using solvent peak as internal standard. Coupling constants (J) are in Hz. Infrared spectral data was obtained on a Thermo Scientific Nicolet 380 FT-IR spectrometer as thin films on ZnSe disks and peaks are reported in cm^{-1}. Electrospray ionization mass spectrometry (ESI-MS) was recorded on a Waters Q-TOF Premier mass spectrometer. Elemental Analysis was performed on a Vario microcube Elementar Analyzer. Reaction progress was monitored by thin-layer chromatography on silica gel plates (60-F254) and observed under UV light. UV−vis titrations were performed using a Thermo Scientific Evolution UV−vis

spectrophotometer. Column chromatography was performed using silica gel (particle size 40−63 μm).

Methyl (4-Methoxyphenyl) Hydrazinecarbodithioate (2). 4-methoxyphenylhydrazine•HCl (30.00 mmol, 1 equiv) (**1**) was dissolved in 75 mL of ethanol in a round-bottom flask fitted with magnetic stirrer and degassed under nitrogen flow. The solution was stirred for 1 h. Carbon disulfide (34.2 mmol, 2.06 mL) was added dropwise and allowed to stir for 0.5 h. Potassium hydroxide (2.36 g, 42.0 mmol) dissolved in degassed ethanol (25 mL) was then quickly poured into the mixture and the solution was stirred for 0.5 h. Following, methyl iodide (33.60 mmol, 2.09 mL) was added in one aliquot and the solution was stirred for 1 h before concentrating via rotary evaporation. The compound was washed with brine and extracted with ethyl acetate, dried over MgSO$_4$ and concentrated. Column chromatography (9:1 hexane: ethyl acetate) provided **2** (6.012 g, 79%) as a dark brown solid. ^{1}H NMR (300 MHz, Chloroform-*d*) δ 8.64 (br s, 1H, N$_{10}$−H), 6.88−6.84 (m, 4H, Ar H), 5.90 (br s, 1H, N$_{11}$−H), 3.79 (s, 3H, −OCH$_3$), 2.62 (s, 3H, −SCH$_3$). ^{13}C NMR (75 MHz, CDCl$_3$) δ 207.87 (C=S), 155.48 (q, C5), 138.89 (q, C2), 115.25(d, C4 and C6), 114.98(d, C3 and C7), 55.75 (s, -OCH$_3$), 17.54 (s, -SCH$_3$). FTIR (cm^{-1}): 2920 (Ar C−H), 1596 (Ar C=C), 1230 (O−C), 1173 (N−C), 965 (C=S). Anal. Calcd for C$_9$H$_{12}$N$_2$OS$_2$: C, 47.34; H, 5.30; N, 12.27. Found: C, 47.30; H, 5.179; N, 12.17. mp 104 °C.

Pyrrolidine-2-(4-methoxyphenyl)diazothioformamide (3a). (CCDC-2330626). Pyrrolidine (5.5 mmol, 0.459 mL) was added to **2** (5.0 mmol, 1.1416 g), followed by triethylamine (7.0 mmol, 1 mL) and toluene (15 mL). The solution was refluxed under inert conditions for 48 h. The solution was then opened to air after cooling and stirred for 2 h. The solution was washed with brine, extracted with ethyl acetate, dried over MgSO$_4$, and concentrated. The resulting mixture was purified with flash column chromatography 7:3 hexanes: ethyl acetate forming (0.783 g) 63% of dark red solid. The solid was recrystallized with 2:3 ethyl acetate: hexanes to obtain red crystal. ^{1}H NMR (500 MHz, Chloroform-*d*) δ 7.90 (d, *J* = 9.0 Hz, 2H, *o*-Ar H), 6.99 (d, *J* = 9.0 Hz, 2H, *m*-Ar H), 3.96 (t, *J* = 7.2 Hz, 2H, -NCH$_2$), 3.89 (s, 3H, -OCH$_3$), 3.65 (t, *J* = 7.2 Hz, 2H, -NCH$_2$), 2.07−2.03 (m, 4H, 2-NCH$_2$CH$_2$). ^{13}C NMR (126 MHz, CDCl$_3$) δ 191.34 (C=S), 163.75 (q, C5), 146.30 (q, C2), 126.21 (d, C3 and C7), 114.48 (d, C4 and C6), 55.82 (s, C12), 53.13 (t, C8), 49.75 (t, C11), 26.32 (t, C9), 24.13 (t, C10). FTIR (cm^{-1}): 3071 (Ar CH), 2977 (Aliphatic CH), 1600 (Ar C=C), 1492 (N=N), 1254 (O−C), 1140 (C−N), 1031 (C=S). MS- ESI (*m/z*): [M + H]$^+$ calcd for C$_{12}$H$_{15}$N$_3$OS, 250.1008; found: 250.1014. mp 62 °C.

Piperidine-2-(4-methoxyphenyl)diazothioformamide (3b) (CCDC-2330627). Piperidine (5.5 mmol, 0.543 mL) was added to **2** (5.0 mmol, 1.1416 g), followed by triethylamine (7.0 mmol, 1 mL) and toluene (15 mL). The solution was refluxed under inert conditions for 48 h. The solution was then opened to air after cooling and stirred for 2 h. The solution was washed with brine, extracted with ethyl acetate, and dried over MgSO$_4$. The concentrated solution was purified with flash column chromatography 7:3 hexane: ethyl acetate forming (0.762 g) 58% of orange solid. Recrystallization with 7:3 ethyl acetate and hexanes provided orange crystals. ^{1}H NMR (500 MHz, Chloroform-*d*) δ 7.88 (d, *J* = 9.0 Hz, 2H, *o*-Ar H), 6.99 (d, *J* = 9.0 Hz, 2H, *m*-Ar H), 4.23 (t, *J* = 5.6 Hz, 2H, -NCH$_2$), 3.89 (s, 3H, -OCH$_3$), 3.60 (t, *J*= 5.6 Hz, 2H, -NCH$_2$), 1.85−1.82 (m, 2H, -NCH$_2$CH$_2$), 1.76−1.72 (m, 2H, - NCH$_2$CH$_2$), 1.66−1.61

(m, 2H, - CH$_2$CH$_2$). ^{13}C NMR (126 MHz, CDCl$_3$) δ 193.93 (C=S), 163.58 (q, C5), 146.34 (q, C2), 126.04 (d, C3 and C7), 114.49 (d, C4 and C6), 55.84 (s, -OCH$_3$), 51.28 (t, C9), 49.54 (t, C13), 26.29 (t, C10), 25.53 (t, C12), 24.28 (t, C11). FTIR (cm^{-1}): 3006 (Ar CH), 2953 (Aliphatic CH), 1602 (Ar C=C), 199 (N=N), 1254 (O−C), 1153 (C−N), 1004 (C=S). MS- ESI (*m/z*): [M + H]$^+$ calcd for C$_{13}$H$_{17}$N$_3$OS, 264.1158; found: 264.1171. mp 92 °C.

N-Methyl Piperizine-2-(4-methoxyphenyl)-diazothioformamide (3c) (CCDC-2330632). N-methyl piperazine (5.5 mmol, 0.659 mL) was added to **2** (5.0 mmol, 1.1416 g) followed by triethylamine (7.0 mmol, 1.0 mL) and toluene (15 mL). The solution was refluxed under inert condition for 48 h. The dark red solution was opened to the air, after cooling, and stirred for 2 h. The solution was washed with brine, extracted with ethyl acetate, and dried over MgSO$_4$. Column chromatography (2:3 hexane: ethyl acetate) of the concentrated mixture produced (0.803 g) 58% of a red solid. Recrystallization in ethyl acetate afforded red crystals. ^{1}H NMR (500 MHz, Chloroform-*d*) δ 7.85 (d, *J* = 9.1 Hz, 2H, *o*-Ar H), 6.95 (d, *J* = 9.1 Hz, 2H, *m*-Ar H), 4.28 (t, *J* = 5.2 Hz, 2H, -NCH$_2$), 3.85 (s, 3H, -OCH$_3$), 3.68 (t, *J* = 5.1 Hz, 2H, -NCH$_2$), 2.59 (t, *J* = 5.2 Hz, 2H, -N(CH$_3$)CH$_2$), 2.41 (t, *J* = 5.1 Hz, 2H, -N(CH$_3$)CH$_2$), 2.30 (s, 3H, -NCH$_3$). ^{13}C NMR (126 MHz, CDCl$_3$) δ 194.26 (C=S), 163.66 (q, C5), 146.15 (q, C2), 126.04 (d, C3 and C7), 114.43 (d, C4 and C6), 55.76 (s, -OCH$_3$), 54.46 (t, C8), 54.13 (t, C10), 49.58 (t, C9), 47.99 (t, C11), 45.72 (s, -NCH$_3$). FTIR (cm^{-1}): 2926 (Ar CH), 1603 (Ar C=C), 1459 (N=N), 1297 (O−C), 1140 (C−N), 1037 (C=S). MS- ESI (*m/z*): [M + H]$^+$ calcd for C$_{13}$H$_{18}$N$_4$OS, 279.1277; found: 279.1280. mp 103 °C.

Morpholine-2-(4-methoxyphenyl)diazothioformamide (3d) (CCDC-2330628). Morpholine (5.5 mmol, 0.474 mL) was added to **2** (5.0 mmol, 1.1416 g), followed by triethylamine (7.0 mmol, 1 mL) and toluene (15 mL). The solution was refluxed under inert conditions for 48 h. The solution was opened to the air, after cooling, and stirred for an additional 2 h. The solution was then washed with brine, extracted with ethyl acetate, and dried over MgSO$_4$. The concentrated solution was purified with flash column chromatography 7:3 hexane: ethyl acetate forming (0.793 g) 60% of a shiny dark red solid. Recrystallization in methanol afforded red crystals. ^{1}H NMR (500 MHz, Chloroform-*d*) δ 7.88 (d, *J* = 9.0 Hz, 2H, *o*-Ar H), 6.98 (d, *J* = 9.0 Hz, 2H, *m*-Ar H), 4.30 (t, *J* = 5.1 Hz, 2H, -NCH$_2$), 3.89 (t, *J* = 5 Hz, 2H, -OCH$_2$), 3.88 (s, 3H, -OCH$_3$), 3.74−3.70 (m, 4H, -NCH$_2$CH$_2$O−). ^{13}C NMR (126 MHz, CDCl$_3$) δ 194.51 (C=S), 163.91 (q, C5), 146.25 (q, C2), 126.28 (d, C3 and C7), 114.54 (d, C4 and C6), 66.45 (t, C9), 66.26 (t, C11), 55.84 (s, -OCH$_3$), 49.91 (t, C8), 48.75 (t, C10). FTIR (cm^{-1}): 2969 (Ar CH), 1595 (Ar C=C), 1497 (N=N), 1272 (O−C), 1110 (C−N), 1010 (C=S). MS- ESI (*m/z*): [M + H]$^+$ calcd for C$_{12}$H$_{15}$N$_3$O$_2$S, 266.0950; found: 266.0963. mp 79 °C.

General Procedure A [ATF•Cu(l)X]$_2$. To ligands **3a** - **3d** (0.40 mmol, 1 equiv) dissolved in 5 mL of anhydrous acetonitrile was added Cu(I)Br (0.40 mmol, 57 mg) or Cu(I)I (0.40 mmol, 76 mg) in one portion. The solution produced a rapid color change and was stirred for 1 h at 50 °C to promote solvation. After cooling, the solvent was evaporated using rotatory evaporator and the dried solid was then washed with hexanes to remove excess ligand.

General Procedure B [Cu(l)(ATF)$_2$]BF$_4$. To ligands **3a** - **3d** (0.40 mmol, 2 equiv) dissolved in 5 mL of anhydrous

acetonitrile was added [(CH$_3$CN)$_4$Cu(I)]BF$_4$ (0.20 mmol, 62 mg). The solution had a rapid color change and was stirred for 1 h at 50 °C to promote further solvation. After cooling, the solvent was evaporated using rotatory evaporator and the dried solid was washed with hexanes to remove excess ligand.

Pyrrolidine-2-(4-methoxyphenyl)diazothioformamide − Cu(l)BF$_4$ (4a) (CCDC-2330630). General Procedure B was followed to give 168 mg of a dark green crystalline solid (63%) ^{1}H NMR (500 MHz, DMSO-d_6) δ 7.93 (br s, 4H, *o*-Ar H), 7.20 (d, *J* = 8.6 Hz, 4H, *m*-Ar H), 4.54 (br s, 4H, 2-NCH$_2$), 4.25 (br s, 4H, 2-NCH$_2$), 3.92 (s, 6H, 2-OCH$_3$), 2.16−2.12 (m, 8H, 4-NCH$_2$CH$_2$). ^{13}C NMR (126 MHz, DMSO) δ 182.81 (C=S), 166.97 (q, C5), 145.70 (br q, C2), 129.69 (d, C3 and C7), 115.54 (d, C4 and C6), 56.48 (s, -OCH$_3$), 54.44 (t, C8), 52.63 (t, C11), 25.13 (t, C9), 23.81 (t, C10). FTIR (cm^{-1}): 2963 (Ar CH), 1588 (Ar C=C), 1438 (N=N), 1269 (O−C), 1139 (C−N), 1080 (C=S). Anal. Calcd for C$_{24}$H$_{30}$BCuF$_4$N$_6$O$_2$S$_2$$^-$: C, 44.42; H, 4.66; N, 12.95. Found: C, 44.12; H, 4.285; N, 12.60. mp 202 °C.

Pyrrolidine-2-(4-methoxyphenyl)diazothioformamide − Cu(l)I (4b). General Procedure A was followed to give 255 mg of a dark green solid (70%). ^{1}H NMR (300 MHz, DMSO-d_6) δ 8.34 (d, *J* = 8.6 Hz, 4H, *o*-Ar H), 7.16 (d, *J* = 8.6 Hz, 4H, *m*-Ar H), 4.25 (br s, 4H, 2-NCH$_2$), 3.91 (s, 6H, 2-OCH$_3$), 3.83 (br s, 4H, 2-NCH$_2$), 2.12 (br s, 8H, 4-NCH$_2$CH$_2$). ^{13}C NMR (75 MHz, DMSO) δ 182.93 (C=S), 165.97 (q, C5), 144.33 (q, C2), 129.41 (d, C3 and C7), 115.73 (d, C4 and C7), 56.40 (s, -OCH$_3$), 54.49 (t, C8), 52.42 (t, C11), 25.10 (t, C9), 23.71 (t, C10). FTIR (cm^{-1}): 2938 (Ar C=C), 1436 (N=N), 1268 (O−C), 1112 (C−N), 1072 (C=S). Anal. Calcd for C$_{24}$H$_{30}$I$_2$Cu$_2$N$_6$O$_2$S$_2$: C, 32.77; H, 3.44; N, 9.55. Found: C, 32.49; H, 3.525; N, 9.27. mp 192 °C.

Pyrrolidine-2-(4-methoxyphenyl)diazothioformamide − Cu(l)Br (4c). General Procedure A was followed to give 135 mg of a dark green solid (42%). ^{1}H NMR (300 MHz, DMSO-d_6) δ 8.37 (d, *J* = 8.8 Hz, 4H, *o*-Ar H), 7.17 (d, *J* = 8.8 Hz, 4H, *m*-Ar H), 4.23 (br s, 4H, 2-NCH$_2$), 3.91 (s, 6H, 2-OCH$_3$), 3.82 (br s, 4H, 2-NCH$_2$), 2.16−2.08 (m, 8H, 4-NCH$_2$CH$_2$). ^{13}C NMR (75 MHz, DMSO) δ 182.96 (C=S), 165.98 (q, C5), 144.44 (q, C2), 129.26 (d, C3 and C7), 115.81 (d, C4 and C6), 56.40 (s, -OCH$_3$), 54.53 (t, C8), 52.46 (t, C11), 25.09 (t, C9), 23.71 (t, C10). FTIR (cm^{-1}): 2971 (Ar CH), 1593 (Ar C=C), 1436 (N=N), 1265 (O−C), 1139 (C−N), 1066 (C=S). Anal. Calcd for C$_{24}$H$_{30}$Br$_2$Cu$_2$N$_6$O$_2$S$_2$: C, 36.70; H, 3.85; N, 10.70. Found: C, 36.60; H, 3.745; N, 10.82. mp 161 °C.

Piperidine-2-(4-methoxyphenyl)diazothioformamide − Cu(l)BF$_4$ (5a) (CCDC-2330629). General Procedure B was followed to give 189 mg of a dark green crystalline material (72%). ^{1}H NMR (300 MHz, Chloroform-*d*) δ 8.09 (d, *J* = 8.8 Hz, 4H, *o*-Ar H), 6.98 (d, *J* = 8.8 Hz, 4H, *m*-Ar H), 4.51 (br s, 4H, 2-NCH$_2$), 4.30 (br s, 4H, 2-NCH$_2$), 3.89 (s, 6H, 2-OCH$_3$), 1.95−1.89 (m, 12H, 6-NCH$_2$CH$_2$CH$_2$). ^{13}C NMR (75 MHz, CDCl$_3$) δ 186.87 (C=S), 167.20 (q, C5), 145.32 (q, C2), 129.83 (d, C3 and C7), 116.11 (d, C4 and C6), 56.62 (s, -OCH$_3$), 54.35 (t, C9), 51.95 (t, C13), 27.21 (t, C10), 26.13 (t, C12), 24.12 (t, C11). FTIR (cm^{-1}): 2942 (Ar CH), 1589 (Ar C=C), 1438 (N=N), 1264 (O−C), 1114 (C−N), 1047 (C=S). Anal. Calcd for C$_{26}$H$_{34}$BCuF$_4$N$_6$O$_2$S$_2$$^-$: C, 46.12; H, 5.06; N, 12.41. Found: C, 46.40; H, 4.942; N, 12.37. mp 201 °C.

Piperidine-2-(4-methoxyphenyl)diazothioformamide − Cu(l)I (5b). General Procedure A was followed to give 232

mg of a dark green solid (65%). ^{1}H NMR (500 MHz, Chloroform-*d*) δ 8.46 (d, *J* = 8.7 Hz, 4H, *o*-Ar H), 7.04 (d, *J* = 8.7 Hz, 4H, *m*-Ar H), 4.43 (br s, 4H, 2-NCH$_2$), 4.33−4.31 (m, 4H, 2-NCH$_2$), 3.94 (s, 6H, 2-OCH$_3$), 1.94 (t, *J* = 4.9 Hz, 4H, 2-NCH$_2$CH$_2$), 1.87−1.86 (m, 8H, 4-NCH$_2$CH$_2$CH$_2$). ^{13}C NMR (126 MHz, CDCl$_3$) δ 187.89 (C=S), 166.60 (q, C5), 145.56 (q, C2), 130.17 (d, C3 and C7), 115.82 (d, C4 and C6), 56.54 (s, -OCH$_3$), 54.21 (t, C9), 51.54 (t, C13), 27.19 (t, C10), 26.02 (t, C12), 24.30 (t, C11). FTIR (cm^{-1}): 2935 (Ar CH), 1596 (Ar C=C), 1436 (N=N), 1264 (O−C), 1109 (C−N), 1022 (C=S). Anal. Calcd for C$_{26}$H$_{34}$I$_2$Cu$_2$N$_6$O$_2$S$_2$: C, 34.41; H, 3.78; N, 9.26. Found: C, 34.25; H, 3.725; N, 9.46. mp 187 °C.

Piperidine-2-(4-methoxyphenyl)diazothioformamide − Cu(l)Br (5c) (CCDC-2330631). General Procedure A was followed to give 148 mg of a dark green crystalline solid (46%). ^{1}H NMR (500 MHz, Chloroform-*d*) δ 8.55 (d, *J* = 8.7 Hz, 4H, *o*-Ar H), 7.04 (d, *J* = 8.7 Hz, 4H, *m*-Ar H), 4.41 (br s, 4H, 2-NCH$_2$), 4.33 (t, *J* = 5.7 Hz, 4H, 2-NCH$_2$), 3.94 (s, 6H, 2-OCH$_3$), 1.96−1.94 (m, 4H, 2-NCH$_2$CH$_2$), 1.86 (dt, *J* = 5.7, 3.0 Hz, 8H, 4-NCH$_2$CH$_2$CH$_2$). ^{13}C NMR (126 MHz, CDCl$_3$) δ 188.13 (C=S), 166.90 (q, C5), 145.40 (q, C2), 130.49 (d, C3 and C7), 115.85 (d, C4 and C6), 56.47 (s, -OCH$_3$), 54.63 (t, C9), 51.58 (t, C13), 27.24 (t, C10), 26.07 (t, C12), 24.28 (t, C11). FTIR (cm^{-1}): 2940 (Ar CH), 1592 (Ar C=C),1437 (N=N), 1265 (O−C), 1147 (C−N), 1048 (C=S). Anal. Calcd for C$_{26}$H$_{34}$Br$_2$Cu$_2$N$_6$O$_2$S$_2$: C, 38.38; H, 4.21; N, 10.33. Found: C, 37.96; H, 4.33; N, 10.21. mp 190 °C.

N-Methyl Piperizine-2-(4-methoxyphenyl)-diazothioformamide − Cu(l)BF$_4$ (6a). General Procedure B was followed to give 158 mg of a dark green solid (61%). ^{1}H NMR (500 MHz, Acetonitrile-d_3) δ 8.55 (d, *J* = 9.1 Hz, 4H, *o*-Ar H), 7.11 (d, *J* = 9.1 Hz, 4H, *m*-Ar H), 4.37 (t, *J* = 5.2 Hz, 4H, 2-NCH$_2$), 4.26 (t, *J* = 5.3 Hz, 4H, 2-NCH$_2$), 3.94 (s, 6H, 2-OCH$_3$), 2.64 (t, *J* = 5.3 Hz, 4H, 2-NCH$_2$CH$_2$), 2.58 (t, *J* = 5.2 Hz, 4H, 2-NCH$_2$CH$_2$), 2.32 (s, 6H, 2-NCH$_3$). ^{13}C NMR (126 MHz, CD$_3$CN) δ 188.87 (C=S), 167.30 (q, C5), 146.15 (q, C2), 130.64 (d, C3 and C7), 116.47 (d, C4 and C6), 57.17 (s, -OCH$_3$), 55.56 (t, C8), 54.61 (t, C11), 53.16 (t, C9), 50.72 (t, C10), 45.56 (s, -NCH$_3$). FTIR (cm^{-1}): 2936 (Ar CH), 1670 (Ar C=C), 1437 (N=N), 1253 (O−C), 1139 (C−N), 1018 (C=S). Anal. Calcd for C$_{26}$H$_{36}$BCuF$_4$N$_8$O$_2$S$_2$$^-$: C, 44.16; H, 5.13; N, 15.85. Found: C, 43.35; H, 5.260; N, 15.73. mp 175 °C.

N-Methyl Piperizine-2-(4-methoxyphenyl)-diazothioformamide − Cu(l)I (6b). General Procedure A was followed to give 244 mg of a dark green solid (70%). ^{1}H NMR (300 MHz, DMSO-d_6) δ 8.43 (br s, 4H, Ar H), 7.21 (d, *J* = 8.7 Hz, 4H, Ar H), 4.45 (br s, 4H, 2-NCH$_2$), 4.30 (br s, 4H, 2-NCH$_2$), 3.94 (s, 6H, 2-OCH$_3$), 2.64−2.58 (m, 8H, 4-NCH$_2$CH$_2$), 2.29 (s, 6H, 2-NCH$_3$). ^{13}C NMR (75 MHz, DMSO) δ 186.69 (C=S), 166.07 (q, C5), 143.95 (q, C2), 129.62 (d, C3 and C7), 115.62 (d, C4 and C6), 56.41 (s, -OCH$_3$), 54.43 (t, C8), 53.56 (t, C11), 51.81 (t, C9), 49.52 (t, C10), 44.85 (s, -NCH$_3$). FTIR (cm^{-1}): 2927 (Ar CH), 1603 (Ar C=C), 1436 (N=N), 1266 (O−C), 1141 (C−N), 1064 (C=S). Anal. Calcd for C$_{26}$H$_{36}$I$_2$Cu$_2$N$_8$O$_2$S$_2$: C, 33.31; H, 3.87; N, 11.95. Found: C, 33.2; H, 3.97; N, 11.32. mp 172 °C.

N-Methyl Piperizine-2-(4-methoxyphenyl)-diazothioformamide − Cu(l)Br (6c). General Procedure A was followed to give 138 mg of a dark green solid (44%). ^{1}H NMR (300 MHz, Acetonitrile-d_3) δ 8.32 (d, *J* = 9.2 Hz, 4H, *o*-Ar H), 7.05 (d, *J* = 9.2 Hz, 4H, *m*-Ar H), 4.41 (t, *J* = 5.2 Hz,

4H, 2-NCH$_2$), 4.27 (t, J = 5.2 Hz, 4H, 2-NCH$_2$), 3.91 (s, 6H, 2-OCH$_3$), 2.62 (br s, 8H, 2-NCH$_2$CH$_2$), 2.33 (s, 6H, 2-NCH$_3$). ^{13}C NMR (75 MHz, CDCl$_3$) δ 188.97 (C=S), 167.53 (q, C5), 146.15 (q, C2), 130.46 (q, C3 and C7), 116.55 (d, C4 and C6), 57.21 (s, -OCH$_3$), 55.55 (t, C8), 54.63 (t, C11), 53.20 (t, C9), 50.94 (t, C10), 45.53 (s, -NCH$_3$). FTIR (cm^{-1}): 2923 (Ar CH), 1670 (Ar C=C), 1458 (N=N), 1287 (O−C), 1152 (C−N), 1065 (C=S). Anal. Calcd for C$_{26}$H$_{36}$Br$_2$Cu$_2$N$_8$O$_2$S$_2$: C, 37.02; H, 4.30; N, 13.28. Found: C, 37.36; H, 4.174; N, 13.47. mp 140 °C.

Morpholine-2-(4-methoxyphenyl)diazothioformamide − Cu(I)BF$_4$ (7a). General Procedure B was followed to give 197 mg of a dark green solid (75%). ^{1}H NMR (500 MHz, Acetonitrile-d_3) δ 8.17 (d, J = 9.2 Hz, 4H, o-Ar H), 7.02 (d, J = 9.2 Hz, 4H, m-Ar H), 4.46 (t, J = 4.9 Hz, 4H, 2-NCH$_2$), 4.29 (dd, J = 5.5, 4.9 Hz, 4H, 2-OCH$_2$), 3.94−3.92 (m, 4H, 2-NCH$_2$), 3.90 (s, 6H, 2-OCH$_3$), 3.89−3.87 (m, 4H, 2-OCH$_2$). ^{13}C NMR (126 MHz, CD$_3$CN) δ 189.24 (C=S), 167.87 (q, C5), 146.02 (q, C2), 130.40 (d, C3 and C7), 116.64 (d, C4 and C6), 67.37 (t, C9), 66.67 (t, C10), 57.25 (s, -OCH$_3$), 53.53 (t, C8), 51.77 (t, C11). FTIR (cm^{-1}): 2930 (Ar CH), 1590 (Ar C=C), 1440 (N=N), 1266 (O−C), 1147 (C−N), 1029 (C=S). Anal. Calcd for C$_{24}$H$_{30}$BCuF$_4$N$_6$O$_4$S$_2^-$: C, 42.33; H, 4.44; N, 12.34. Found: C, 42.27; H, 4.954; N, 12.36. mp 186 °C.

Morpholine-2-(4-methoxyphenyl)diazothioformamide − Cu(I)I (7b). General Procedure A was followed to give 264 mg of a dark green solid (70%). ^{1}H NMR (300 MHz, Acetonitrile-d_3) δ 7.86 (d, J = 9.1 Hz, 4H, o-Ar H), 7.08 (d, J = 9.1 Hz, 4H, m-Ar H), 4.22 (t, J = 5.0 Hz, 4H, 2-NCH$_2$), 3.89 (s, 6H, 2-OCH$_3$), 3.83 (t, J = 5.0 Hz, 4H, 2-NCH$_2$), 3.72−3.64 (m, 8H, 4-OCH$_2$). ^{13}C NMR (75 MHz, CD$_3$CN) δ 194.81 (C=S), 165.04 (q, C5), 146.85 (q, C2), 126.83 (d, C3 and C7), 115.73 (d, C4 and C6), 66.81 (t, C9 and C10), 56.67 (s, -OCH$_3$), 50.71 (t, C8), 49.81 (t, C11). FTIR (cm^{-1}): 2904 (Ar CH), 1601 (Ar C=C), 1454 (N=N), 1245 (O−C), 1174 (C−N), 1029 (C=S). Anal. Calcd for C$_{24}$H$_{30}$I$_2$Cu$_2$N$_6$O$_4$S$_2$: C, 31.62; H, 3.32; N, 9.22. Found: C, 31.95; H, 3.693; N, 9.14. mp 205 °C.

Morpholine-2-(4-methoxyphenyl)diazothioformamide − Cu(I)Br (7c). General Procedure A was followed to give 153 mg of a dark green solid (45%). ^{1}H NMR (300 MHz, Acetonitrile-d_3) δ 7.94 (d, J = 9.1 Hz, 4H, o-Ar H), 7.08 (d, J = 9.1 Hz, 4H, m-Ar H), 4.24−4.21 (m, 4H, 2-NCH$_2$), 3.90 (s, 6H, 2-OCH$_3$), 3.83 (dt, J = 10.0, 5.2 Hz, 8H, 4-NCH$_2$), 3.70−3.67 (m, 4H, 2-OCH$_2$). ^{13}C NMR (75 MHz, CD$_3$CN) δ 190.75 (C=S), 165.41 (q, C5), 146.83 (q, C2), 127.35 (d, C3 and C7), 115.89 (d, C4 and C6), 66.93 (t, C9), 66.78 (t, C10), 56.77 (s, -OCH$_3$), 51.12 (t, C8), 50.09 (t, C11). FTIR (cm^{-1}): 2919 (Ar CH), 1602 (Ar C=C), 1467 (N=N), 1261 (O−C), 1150 (C−N), 1026 (C=S). Anal. Calcd for C$_{24}$H$_{30}$Br$_2$Cu$_2$N$_6$O$_4$S$_2$: C, 35.26; H, 3.70; N, 10.28. Found C, 35.42; H, 3.367; N, 10.18. mp 220 °C.

X-ray Structure Determination. X-ray diffraction data **2330626−2330631** were collected at 100 K on a Bruker D8 Venture using MoKα (λ = 0.71073). X-ray diffraction data for **23330632** were collected on a Bruker SMART APEX II CCD area detector system equipped with a graphite monochromator and a Mo Kα fine-focus sealed tube operated at 1.2 kW power (40 kV, 30 mA). Data have been corrected for absorption using SADABS area detector absorption correction program.[41] Using Olex2, the structure was solved with the SHELXT structure solution program using Direct Methods and refined

with the SHELXL refinement package using least-squares minimization.[42−44] All non-hydrogen atoms were refined with anisotropic thermal parameters. Hydrogen atoms in the investigated structure were located from difference Fourier maps but finally their positions were placed in geometrically calculated positions and refined using a riding model. Isotropic thermal parameters of the placed hydrogen atoms were fixed to 1.2 times the U value of the atoms they are linked to (1.5 times for methyl groups). Hydrogen atoms connected to heteroatoms were located from the difference map, placed, and refined. Calculations and refinement of structures were carried out using APEX4, SHELXTL, and Olex2 software.

UV−Vis Titrations. Cu(I) halides (0.54 mM) were titrated in triplicate from the addition of 0.1 equiv aliquots against 1.2 mL of ATF ligands **3a−d** (0.058 mM) in acetonitrile (ACS grade) until reaching three total equivalents. [CH$_3$CN]$_4$Cu]-BF$_4$ (0.27 mM) was titrated in triplicate adding 0.1 equiv until reaching 1.5 total equivalents. Max absorbance wavelengths were found, and linear regression analysis was calculated over a range of wavelengths (n, n+2, n+4, n-2, n-4) in triplicate using Bindfit freeware and all data is provided utilizing all four types (Full, Additive, Statistical, and noncooperative) of 2:1 binding models.[36] Binding association values are provided in M^{-1} and can be found in Figure S40−42 and **Tables S2−3**.

Computational Studies. All structures were fully optimized without symmetry constraints using the B3LYP functional as implemented in Gaussian09 using the 6-31 G** basis set for C, H, N, S, Br, B, F, and P and the Stuttgart basis set with effective core potentials for all metal and iodine atoms. To verify the validity of the chosen method, other DFT functionals were used: B3LYP-D3, B3P86, B3PW91, M11, and wB97XD, but B3LYP gave structural parameters that best matched the experimental structures. The ultrafine integration grid was employed in all calculations, which ensured the stability of the optimization procedure for the investigated molecules. Each stationary point was confirmed by a frequency calculation at the same level of theory to be a real local minimum on the potential energy surface. More accurate electronic energies were computed for the optimized geometries using the larger 6-311++G(d, p) basis set. All reported free energies are for acetonitrile solution at the standard state (T = 298.15 K, P = 1 atm, 1 mol/L concentration of all species in acetonitrile) as modeled by a polarized continuum model. The energy values given in the manuscript correspond to solvent corrected Gibbs free energies that are based on B3LYP/6-311++G(d,p) electronic energies and all corrections calculated at the B3LYP/6-31 G(d) level.

Cyclic Voltammetry Measurements. Pine research was used for electrochemical investigations at 25 °C. Acetonitrile was employed as solvent, tetrabutylammonium hexafluorophosphate (NBu$_4$PF$_6$) used as the supporting electrolyte; using a three-electrode cell in which a glassy carbon (GC) was the working electrode, an Ag/Ag$^+$ was the reference electrode and a graphite was used as the counter electrode. Cyclic voltammetry was used to characterize the electrochemical behavior of the ligands and their Cu(I) complexes. The scanning potential ranged between −1.8 and 1.8 V (versus Ag/Ag$^+$) with different scan rates 50−500 mVs^{-1}. All experiments were performed under N$_2$ atmosphere, which was achieved by purging the cell solutions with nitrogen gas for approximately 10 min, and the cell solutions were maintained under this atmosphere during the recording of the voltammograms. The glassy carbon electrode was polished with fine alumina powder

on wet polishing cloth for approximately 5 min. The shiny, mirror-like electrode surface was then thoroughly washed with distilled water.

Antimicrobial Microtiter Assay. Antimicrobial assays were conducted as previously described.[12] Briefly, ATF or ATF-metal complexes were weighed out using an analytical scale in a sterile environment and were dissolved in 100% ethanol to make a 10 mM stock that was stored at 2−8 °C for less than 1 week. Stability testing (over 48 h) via UV−vis was conducted for complexes and are shown in ESI (Figure S79−81). From the 10 mM stock, drug dilutions were prepared and added to sterile nontissue culture treated 96-well plates to produce a range of final concentrations from 1 to 100 μM. The microbes used in this study were: *E. coli* [ATCC 8739], *Staphylococcus aureus* [ATCC BAA-44, MRSA], and *Candida albicans* [ATCC 10213]. Microbial cultures grown on Mueller-Hinton (MH) agar, pH 7.2 (for *E. coli* and *Staphylococcus aureus*), or Yeast-Peptone-Dextrose (YPD) agar, pH 6.5 (for *Candida albicans*). For experiments, 5 mL cultures of MH broth, pH 7.2 (*E. coli*), or MH broth +2% NaCl, pH 7.2 (*Staphylococcus aureus*), or YPD broth, pH 6.8 (*Candida albicans*) were prepared by inoculating with colonies grown on the respective agar plates. The cultures were incubated at 37 °C with shaking (220 rpm) for 2−4 h to achieve a 0.5 McFarland Standard ($OD_{600\,nm}$ = 0.08−0.10). The culture was then diluted 1:200 into the respective fresh media and added to the plate containing the drug dilutions. The plates were incubated at 37 °C in a humidified incubator, and the absorbance at 600 nm measured at 24 h using a BioTek Synergy HT multiwell plate reader. All drug concentrations were tested in quadruplicate, and all experiments were repeated 2−3 times. Chloramphenicol (2.5 mg/mL) was used as a negative control (no growth was observed with this treatment). Solvent controls consisted of wells treated with ethanol at concentrations up to 1% (no inhibition of growth was observed with ethanol ≤1%). Kanamycin, ampicillin, and ketoconazole were used as drug comparison controls. The minimal inhibitory concentration (MIC) was recorded in micromolar and defined as the lowest tested drug concentration that produced no microbial growth. The half maximal inhibitory concentration (IC_{50}) was calculated using the following equations:

$$Average\ absorbance\ (600\ nm,\ 24\ h) = \bar{x} absorbance\ of\ test\ drug\ conc - \bar{x} absorbance\ 0\ h\ control$$

$$\%\ max\ Growth = \frac{\bar{x} absorbance\ of\ test\ drug\ conc - \bar{x} absorbance\ negative\ control}{\bar{x} absorbance\ of\ positive\ untreated\ control - \bar{x} absorbance\ negative\ control}$$

The normalized max growth values were plotted as a function of the logarithmic drug concentration using GraphPad Prism (version 6) software. The IC_{50} was calculated using a nonlinear regression fit using GraphPad Prism and ± standard error mean (SEM) of several experiments was calculated in Microsoft Excel. While drug concentrations up to 100 μM were tested for all compounds, IC_{50} values above 50 μM were simply reported as >50 μM.

Mammalian Cell Microtiter Assay. Antiproliferative assays were conducted as previously described,[12] using tissue culture treated sterile 96-well plates. Briefly, the normal and cancer cell lines examined in this study were all human: A549 lung carcinoma [ATCC CCL-185], HT-1080 fibrosarcoma [ATCC CCL-121], breast carcinoma MDA-MB-231 [ATCC HTB-26], lymphoblastic leukemia K-562 [ATCC CCL-243], normal

lung epithelial MRC-5 [ATCC CCL-171], and normal human foreskin fibroblast HFF [Millipore Sigma: SCC058]. Cells were cultured in their respective media: DMEM/F12 (A549), DMEM (MDA-MB-231; HFF), EMEM (HT-1080, MRC-5), or IMDM (K-562) supplemented with 10% cosmic calf serum (CCS) and grown at 37 °C in a 5% CO_2 atmosphere. Adherent cells (all except K562) were plated at 5,000 cells/180 μL media and allowed to adhere for 24 h before addition of drug. The nonadherent K562 line was plated at 5,000 cells/well, and drug added on the same day as plating. Dilutions of 10 mM ATF or ATF-metal chelate stock solutions were made in media containing serum. Drugs were tested at concentrations from 0.1 to 100 μM in quadruplicate and assays were repeated 2−3 times. After 48 h of drug exposure, 20 μL of sterile 0.1% resazurin in phosphate buffered saline was added to each well. Living, metabolically active cells convert blue resazurin to fluorescent pink resorufin. After 24−48 h (depending on cell type) fluorescence was measured using a BioTek Synergy HT multiwell plate reader (excitation 530 nm/emission 590 nm). Wells treated with 15% dimethyl sulfoxide (DMSO) were used to establish the background fluorescence for the assay (100% cell death). Dilutions of ethanol were used as solvent controls for the experiment (no inhibition of growth was seen up to 1%, the highest concentration used in an experiment). Cisplatin was used as a drug comparison control. The IC_{50} (±SEM) values for cisplatin activity across all cell lines were A549 = 19.0 μM (±0.6); HT-1080 = 17.5 (±0.1); MDA-MB-231 = 48.6 μM (±0.9); K-562 = 18.5 μM (±1.0); MRC-5 = 33.7 μM (±0.6); HFF > 50 μM. The percent cell viability was calculated from the following equation:

$$\%\ Cell\ Viability = \frac{\bar{x}\ drug\ treatment\ concentration\ fluorescence - \bar{x}\ negative\ control\ fluorescence}{\bar{x}\ positive\ (untreated)\ control\ fluorescence - \bar{x}\ negative\ control\ fluorescence}$$

The normalized cell viability values were plotted as a function of the logarithmic drug concentration using GraphPad Prism (version 6) software. The IC_{50} was calculated using a nonlinear regression fit using GraphPad Prism and ± standard error mean (SEM) was calculated from independent experiments using Microsoft Excel.

■ ASSOCIATED CONTENT

Ⓢ Supporting Information

The Supporting Information is available free of charge at https://pubs.acs.org/doi/10.1021/acsomega.4c04216.

> Pyrrolidine-2-(4-methoxyphenyl)diazothioformamide (**3a**) (CIF)
>
> Piperidine-2-(4-methoxyphenyl) diazothioformamide (**3b**) (CIF)
>
> Morpholine-2-(4-methoxyphenyl) diazothioformamide (**3d**)(CIF)
>
> *N*-methyl piperizine-2-(4-methoxyphenyl) diazothioformamide (**3c**) (CIF)
>
> Pyrrolidine-2-(4-methoxyphenyl) diazothioformamide − Cu(l)BF4 (**4a**) (CIF)
>
> Piperidine-2-(4-methoxyphenyl) diazothioformamide − Cu(l)BF4 (**5a**) (CIF)
>
> Piperidine-2-(4-methoxyphenyl) diazothioformamide − Cu(l)Br (**5c**) (CIF)
>
> ^{1}H and ^{13}C NMR spectral data are shown in Figures S1−S34; Figures S35−38 provide Mass Spec data; UV−vis and binding data can be found in Figures S39−S42

and Tables S1–S3; computational data can be found in Figures S50–S52 and Table 5; X-ray structures and experimental can be found in Figures S43–S49 and Table S4; cyclic voltammetry is found in Figures S53–S56 and Table S6; FTIR spectral data are found in Figures S57–S72; NMR spectra for stability test of complexes are found in Figures S73–S76; UV–vis spectra for stability test of complexes are found in Figures S77–S79; and MIC data in Table S7 (PDF)

AUTHOR INFORMATION

Corresponding Authors

Kenneth A. Cornell − *Department of Chemistry and Biochemistry, Boise State University, Boise, Idaho 83725, United States*; Email: kencornell@boisestate.edu

Kristopher V. Waynant − *Department of Chemistry, University of Idaho, Moscow, Idaho 83844, United States*; orcid.org/0000-0002-4096-5726; Email: kwaynant@uidaho.edu

Authors

Laxmi Tiwari − *Department of Chemistry, University of Idaho, Moscow, Idaho 83844, United States*

Caleb Leach − *Department of Chemistry and Biochemistry, Boise State University, Boise, Idaho 83725, United States*

Ashley Williams − *Department of Chemistry and Biochemistry, Boise State University, Boise, Idaho 83725, United States*

Brandon Lighter − *Department of Chemistry and Biochemistry, Boise State University, Boise, Idaho 83725, United States*

Zachariah Heiden − *Department of Chemistry, Washington State University, Pullman, Washington 99164, United States*; orcid.org/0000-0002-7192-4441

Mark F. Roll − *Department of Mechanical Engineering, University of Idaho, Moscow, Idaho 83844, United States*; orcid.org/0000-0003-4701-1922

James G. Moberly − *Department of Chemical and Biological Engineering, University of Idaho, Moscow, Idaho 83844, United States*; orcid.org/0000-0003-0950-0952

Complete contact information is available at:
https://pubs.acs.org/10.1021/acsomega.4c04216

Notes

The authors declare no competing financial interest.

REFERENCES

(1) Ufnalska, I.; Drew, S. C.; Zhukov, I.; Szutkowski, K.; Wawrzyniak, U. E.; Wróblewski, W.; Fraczyk, T.; Bal, W. Intermediate Cu(II)-Thiolate Species in the Reduction of Cu(II)GHK by Glutathione: A Handy Chelate for Biological Cu(II) Reduction. *Inorg. Chem.* **2021**, *60* (23), 18048−18057.

(2) Festa, R. A.; Thiele, D. J. Copper: An essential metal in biology. *Curr. Biol.* **2011**, *21* (21), R877−R883.

(3) Santini, C.; Pellei, M.; Gandin, V.; Porchia, M.; Tisato, F.; Marzano, C. Advances in Copper Complexes as Anticancer Agents. *Chem. Rev.* **2014**, *114* (1), 815−862.

(4) Gupte, A.; Mumper, R. J. Elevated copper and oxidative stress in cancer cells as a target for cancer treatment. *Cancer Treat Rev.* **2009**, *35* (1), 32−46.

(5) Yuan, J.; Lovejoy, D. B.; Richardson, D. R. Novel di-2-pyridyl-derived iron chelators with marked and selective antitumor activity: in vitro and in vivo assessment. *Blood* **2004**, *104* (5), 1450−1458.

(6) Singh, V.; Palakkeezhillam, V. N. V.; Manakkadan, V.; Rasin, P.; Valsan, A. K.; Kumar, V. S.; Sreekanth, A. Recent developments on the potential biological applications of transition metal complexes of thiosemicarbazone derivatives. *Polyhedron* **2023**, *245*, 116658.

(7) Bajaj, K.; Buchanan, R. M.; Grapperhaus, C. A. Antifungal activity of thiosemicarbazones, bis(thiosemicarbazones), and their metal complexes. *J. Inorg. Biochem* **2021**, *225*, 111620.

(8) Palanimuthu, D.; Shinde, S. V.; Somasundaram, K.; Samuelson, A. G. In Vitro and in Vivo Anticancer Activity of Copper Bis(thiosemicarbazone) Complexes. *J. Med. Chem.* **2013**, *56* (3), 722−734.

(9) Yu, Y.; Kalinowski, D. S.; Kovacevic, Z.; Siafakas, A. R.; Jansson, P. J.; Stefani, C.; Lovejoy, D. B.; Sharpe, P. C.; Bernhardt, P. V.; Richardson, D. R. Thiosemicarbazones from the Old to New: Iron Chelators That Are More Than Just Ribonucleotide Reductase Inhibitors. *J. Med. Chem.* **2009**, *52* (17), 5271−5294.

(10) Li, A. L.; Huang, K.; Pan, W. P.; Wu, Y. R.; Liang, Y. W.; Zhang, Z. L.; Wu, D. Q.; Ma, L. B.; Gou, Y. Thiosemicarbazone Mixed-Valence Cu(I/II) Complex against Lung Adenocarcinoma Cells through Multiple Pathways Involving Cuproptosis. *J. Med. Chem.* **2024**, *67* (11), 9091−9103.

(11) Machado, J. F.; Marques, F.; Pinheiro, T.; de Brito, M. J. V.; Scalese, G.; Pérez-Díaz, L.; Otero, L.; António, J. P. M.; Gambino, D.; Morais, T. S. Copper(I)-Thiosemicarbazone Complexes with Dual Anticancer and Antiparasitic Activity. *Chemmedchem* **2023**, *18* (14), e202300074.

(12) Bai, X. G.; Zheng, Y. Y.; Qi, J. X., Advances in thiosemicarbazone metal complexes as anti-lung cancer agents. *Frontiers in Pharmacology* **2022**, *13*, DOI: 10.3389/fphar.2022.1018951.

(13) Carcelli, M.; Tegoni, M.; Bartoli, J.; Marzano, C.; Pelosi, G.; Salvalaio, M.; Rogolino, D.; Gandin, V. In vitro and in vivo anticancer activity of tridentate thiosemicarbazone copper complexes: Unravelling an unexplored pharmacological target. *Eur. J. Med. Chem.* **2020**, *194*, 112266.

(14) Yuan, J.; Lovejoy, D. B.; Richardson, D. R. Novel di-2-pyridyl-derived iron chelators with marked and selective antitumor activity: in vitro and in vivo assessment. *Blood* **2004**, *104* (5), 1450−1458.

(15) Ritacca, A. G.; Falcone, E.; Doumi, I.; Vileno, B.; Faller, P.; Sicilia, E. Dual Role of Glutathione as a Reducing Agent and Cu-Ligand Governs the ROS Production by Anticancer Cu-Thiosemicarbazone Complexes. *Inorg. Chem.* **2023**, *62* (9), 3957−3964.

(16) Knox, J. J.; Hotte, S. J.; Kollmannsberger, C.; Winquist, E.; Fisher, B.; Eisenhauer, E. A. Phase II study of Triapine in patients with metastatic renal cell carcinoma: a trial of the National Cancer Institute of Canada Clinical Trials Group (NCIC IND.161). *Invest New Drugs* **2007**, *25* (5), 471−7.

(17) Leath, C. A.; Deng, W.; Mell, L. K.; Richardson, D. L.; Walker, J. L.; Holman, L. L.; Lea, J. S.; Amarnath, S. R.; Santos-Reyes, L. J.; Arend, R. C.; Mayadev, J.; Jegadeesh, N.; Disilvestro, P.; Chon, H. S.; Ghamande, S. A.; Quick, A. M.; Chino, J. P.; Mackay, H.; Aghajanian, C.; Monk, B. J. Incorporation of triapine (T) with cisplatin

chemoradiation (CRT) for locally advanced cervical and vaginal cancer: Results from NRG-GY006, a phase III randomized trial. *J. Clin Oncol* **2023**, *41* (16), 5502.

(18) Anjum, R.; Palanimuthu, D.; Kalinowski, D. S.; Lewis, W.; Park, K. C.; Kovacevic, Z.; Khan, I. U.; Richardson, D. R. Synthesis, Characterization, and in Vitro Anticancer Activity of Copper and Zinc Bis(Thiosemicarbazone) Complexes. *Inorg. Chem.* **2019**, *58* (20), 13709−13723.

(19) Palanimuthu, D.; Shinde, S. V.; Somasundaram, K.; Samuelson, A. G. In vitro and in vivo anticancer activity of copper bis(thiosemicarbazone) complexes. *J. Med. Chem.* **2013**, *56* (3), 722−34.

(20) Pradhan, R.; Tiwari, L.; Groner, V. M.; Leach, C.; Lusk, K.; Harrison, N. S.; Cornell, K. A.; Waynant, K. V. Evaluation of azothioformamides and their copper(I) and silver(I) complexes for biological activity. *J. Inorg. Biochem* **2023**, *246*, 112294.

(21) Anjum, R.; Palanimuthu, D.; Kalinowski, D. S.; Lewis, W.; Park, K. C.; Kovacevic, Z.; Khan, I. U.; Richardson, D. R. Synthesis, Characterization, and in Vitro Anticancer Activity of Copper and Zinc Bis(Thiosemicarbazone) Complexes. *Inorg. Chem.* **2019**, *58* (20), 13709−13723.

(22) Peña, Q.; Sciortino, G.; Maréchal, J.-D.; Bertaina, S.; Simaan, A. J.; Lorenzo, J.; Capdevila, M.; Bayón, P.; Iranzo, O.; Palacios, Ò. Copper(II), N,N,O-Chelating Complexes as Potential Anticancer Agents. *Inorg. Chem.* **2021**, *60* (5), 2939−2952.

(23) Leite, C. M.; Honorato, J.; Martin, A. C. B. M.; Silveira, R. G.; Colombari, F. M.; Amaral, J. C.; Costa, A. R.; Cominetti, M. R.; Plutín, A. M.; de Aguiar, D.; Vaz, B. G.; Batista, A. A. Experimental and Theoretical DFT Study of Cu(I)/N,N-Disubstituted-N′-acylthioureato Anticancer Complexes: Actin Cytoskeleton and Induction of Death by Apoptosis in Triple-Negative Breast Tumor Cells. *Inorg. Chem.* **2022**, *61* (1), 664−677.

(24) Besleaga, I.; Stepanenko, I.; Petrasheuskaya, T. V.; Darvasiova, D.; Breza, M.; Hammerstad, M.; Marć, M. A.; Prado-Roller, A.; Spengler, G.; Popović-Bijelić, A.; Enyedy, E. A.; Rapta, P.; Shutalev, A. D.; Arion, V. B. Triapine Analogues and Their Copper(II) Complexes: Synthesis, Characterization, Solution Speciation, Redox Activity, Cytotoxicity, and mR2 RNR Inhibition. *Inorg. Chem.* **2021**, *60* (15), 11297−11319.

(25) Bechgaard, K. Nonplanar Electron-Transfer Complexes.2. Chemistry of 4 Cu-N2s2z Complexes Derived from Copper-Bis-N,N-Diethylphenylazothioformamide. *Acta Chem. Scand A* **1977**, *31a* (8), 683−688.

(26) Nielsen, K. T.; Bechgaard, K.; Krebs, F. C. Effective removal and quantitative analysis of Pd, Cu, Ni, and Pt catalysts from small-molecule products. *Synthesis-Stuttgart* **2006**, *2006* (10), 1639−1644.

(27) Nielsen, K. T.; Harris, P.; Bechgaard, K.; Krebs, F. C. Structural study of four complexes of the M-N2S2 type derived from diethylphenylazothioformamide and the metals palladium, platinum, copper and nickel. *Acta Crystallogr. B* **2007**, *63* (1), 151−156.

(28) Johnson, N. A.; Wolfe, S. R.; Kabir, H.; Andrade, G. A.; Yap, G. P. A.; Heiden, Z. M.; Moberly, J. G.; Roll, M. F.; Waynant, K. V. Deconvoluting the Innocent vs. Non-Innocent Behavior of N,N-Diethylphenylazothioformamide Ligands with Copper Sources. *Eur. J. Inorg. Chem.* **2017**, *2017* (47), 5576−5581.

(29) Pradhan, R.; Groner, V. M.; Gutman, K. L.; Heiden, Z. M.; Roll, M. F.; Moberly, J. G.; Waynant, K. V. Substitution effects on the binding interactions of redox-active arylazothioformamide ligands and copper(I) salts. *Supramol Chem.* **2020**, *32* (8), 466−478.

(30) Pradhan, R.; Groner, V. M.; Gutman, K. L.; Larson, G. E.; Kan, Y.; Zhang, Q.; Heiden, Z. M.; Roll, M. F.; Moberly, J. G.; Waynant, K. V. Evaluating Coordinative Binding Mechanisms through Experimental and Computational Studies of Methoxy-Substituted Arylazothioformamide Copper(I) Complexes. *Eur. J. Inorg. Chem.* **2022**, *2022* (33), No. e202200421.

(31) Pradhan, R.; Groner, V. M.; Johnson, N. A.; Zhang, Q.; Roll, M. F.; Moberly, J. G.; Waynant, K. V. Synthesis of an N, N-diethyl-tert-butylazothioformamide ligand and coordination studies with Copper-(I) salts. *Inorg. Chem. Commun.* **2021**, *124*, 108393.

(32) Wiberg, K. B.; Rablen, P. R. Why Does Thioformamide Have a Larger Rotational Barrier Than Formamide. *J. Am. Chem. Soc.* **1995**, *117* (8), 2201−2209.

(33) Jensen, K. A. B.; et al. Non-Planar Electron-Transfer Complexes Derived from Thiosemicarbazides. New Cation-Stabilized Free Radicals. *Acta Chem. Scand A* **1972**, *26*, 2913−2922.

(34) Tiwari, L.; Waynant, K. V. The synthesis and structural properties of a chloridobis{N-[(4-methoxyphenyl)imino]pyrrolidine-1-carboxamide}zinc(II) (acetonitrile)trichloridozincate coordination complex. *Acta Crystallographica Section E* **2024**, *80* (1), 14−17.

(35) Pradhan, R.; Gutman, K. L.; Ud, A.; Hulley, E. B.; Waynant, K. V. Catalytic Carboxylation of Terminal Alkynes with Copper(I) Azothioformamide Complexes. *Organometallics* **2023**, *42* (5), 362−371.

(36) Thordarson, P. Determining association constants from titration experiments in supramolecular chemistry. *Chem. Soc. Rev.* **2011**, *40* (3), 1305−1323.

(37) Hibbert, D. B.; Thordarson, P. The death of the Job plot, transparency, open science and online tools, uncertainty estimation methods and other developments in supramolecular chemistry data analysis. *Chem. Commun.* **2016**, *52* (87), 12792−12805.

(38) Sigman, D. S.; Mazumder, A.; Perrin, D. M. Chemical nucleases. *Chem. Rev.* **1993**, *93* (6), 2295−2316.

(39) Claudel, M.; Schwarte, J. V.; Fromm, K. M. New Antimicrobial Strategies Based on Metal Complexes. *Chemistry* **2020**, *2* (4), 849−899.

(40) Patra, M.; Wenzel, M.; Prochnow, P.; Pierroz, V.; Gasser, G.; Bandow, J. E.; Metzler-Nolte, N. An organometallic structure-activity relationship study reveals the essential role of a Re(CO)3 moiety in the activity against gram-positive pathogens including MRSA. *Chemical Science* **2015**, *6* (1), 214−224.

(41) Haming, L.; Sheldrick, G. M. Sadabs: A Program for Exploiting the Redundancy of Area-Detector X-Ray Data. *Acta Crystallogr. A* **1999**, *55*, 206−206.

(42) Dolomanov, O. V.; Bourhis, L. J.; Gildea, R. J.; Howard, J. A. K.; Puschmann, H. OLEX2: a complete structure solution, refinement and analysis program. *J. Appl. Crystallogr.* **2009**, *42*, 339−341.

(43) Sheldrick, G. M. SHELXT - Integrated space-group and crystal-structure determination. *Acta Crystallogr. A* **2015**, *71*, 3−8.

(44) Sheldrick, G. M. Crystal structure refinement with SHELXL. *Acta Crystallographica Section C-Structural Chemistry* **2015**, *71*, 3−8.